STUK

STUK-YTO-TR 164 July 2000

# GEOSPHERE TRANSPORT OF RADIONUCLIDES IN SAFETY ASSESSMENT OF SPENT FUEL DISPOSAL

**Petri Jussila**

In STUK this study was supervised by **Esko Eloranta**

**STUK • SÄTEILYTURVAKESKUS • STRÅLSÄKERHETSCENTRALEN**
**RADIATION AND NUCLEAR SAFETY AUTHORITY**

The conclusions presented in the STUK report series are those of the authors and do not necessarily represent the official position of STUK.

ISBN 951-712-395-7
ISSN 0785-9325

Oy Edita Ab, Helsinki 2000

*JUSSILA Petri. Geosphere transport of radionuclides in safety assessment of spent fuel disposal. STUK-YTO-TR 164. Helsinki 2000. 47 pp. + Appendices 18 pp.*

**ISBN** 951-712-395-7
**ISSN** 0785-9325

**Keywords:** geosphere, transport, far-field, migration, radionuclide, safety assessment, spent fuel disposal, nuclear waste, analytical model

# ABSTRACT

The study is associated with a research project of Radiation and Nuclear Safety Authority (STUK) to utilise analytical models in safety assessment for disposal of spent nuclear fuel.

Geosphere constitutes a natural barrier for the possible escape of radionuclides from a geological repository of spent nuclear fuel. However, rock contains fractures in which flowing groundwater can transport material.

Radionuclide transport in rock is complicated - the flow paths in the geosphere are difficult to characterise and there are various phenomena involved. In mathematical models, critical paths along which radionuclides can reach the biosphere are considered. The worst predictable cases and the effect of the essential parameters can be assessed with the help of such models although they simplify the reality considerably.

Some of the main differences between the transport model used and the reality are the mathematical characterisation of the flow route in rock as a smooth and straight fracture and the modelling of the complicated chemical processes causing retardation with the help of a distribution coefficient that does not explain those phenomena.

Radionuclide transport models via a heat transfer analogy and analytical solutions of them are derived in the study. The calculations are performed with a created Matlab® program for a single nuclide model taking into account 1D advective transport along a fracture, 1D diffusion from the fracture into and within the porous rock matrices surrounding the fracture, retardation within the matrices, and radioactive decay.

The results are compared to the results of the same calculation cases obtained by Technical Research Centre of Finland (VTT) and presented in TILA-99 safety assessment report. The model used by VTT is the same but the results have been calculated numerically in different geometry.

The differences between the results of the present study and TILA-99 can to a large extent be explained by the different approaches to employ the rock parameters. Furthermore, the results of the present study are also similar to those presented in TILA-99. Consequently, the results of the present study increase confidence in the results presented in TILA-99.

The effect of varying the values of the rock parameters and the groundwater transit time are found to be significant in some cases. Naturally, the results are the most sensitive for the nuclides that have a small half life compared to the transit time.

*JUSSILA Petri. Radionuklidien kaukoaluekulkeutuminen käytetyn ydinpolttoaineen loppusijoituksen turvallisuustutkimuksessa. STUK-YTO-TR 164. Helsinki 2000. 48 s. + liitteet 17 s.*

**ISBN** 951-712-395-7
**ISSN** 0785-9325

**Avainsanat:** radionuklidi, kaukoaluekulkeutuminen, geosfääri, käytetyn ydinpolttoaineen loppusijoitus, ydinjäte, turvallisuusanalyysi, analyyttinen malli

# TIIVISTELMÄ

Työ on osa Säteilyturvakeskuksen tutkimusprojektia, jossa hyödynnetään analyyttisiä malleja käytetyn ydinpolttoaineen loppusijoituksen turvallisuustutkimuksessa.

Geosfääri muodostaa luonnollisen esteen geologisessa loppusijoitustilassa olevasta käytetystä ydinpolttoaineesta mahdollisesti vapautuville radionuklideille. Kallio kuitenkin sisältää erisuuruisia rakoja, joissa etenemään pääsevällä pohjavedellä on mahdollisuus kuljettaa aineita.

Radionuklidien kulkeutuminen kalliossa on monimutkaista. Kalliossa esiintyvien virtausreittien määrittäminen on vaikeaa ja ongelmaan vaikuttavia ilmiöitä on lukuisia. Matemaattisilla malleilla kuvataan kriittisiä reittejä, joita pitkin radionuklidit saattavat päästä biosfääriin. Vaikka kyseiset mallit yksinkertaistavat todellisuutta huomattavasti, voidaan niiden avulla kuitenkin tutkia pahimpia kuviteltavissa olevia tilanteita sekä arvioida kulkeutumisen kannalta oleellisten parametrien vaikutuksia.

Suurimpia eroavuuksia todellisuuden ja työssä käytetyn mallin välillä ovat kulkeutumisreitin kuvaaminen sileällä ja suoralla raolla sekä pidättymistä aiheuttavien monimutkaisten kemiallisten mekanismien mallintaminen pidätyskertoimella, joka ei selitä pidättymistä aiheuttavia prosesseja.

Työssä johdetaan radionuklidien kulkeutumismalleja lämmönsiirtymisanalogian kautta sekä analyyttisiä ratkaisuja kyseisille malleille. Laskut suoritetaan työtä varten luodulla yksittäisten nuklidien analyyttistä mallia hyödyntävällä Matlab®-ohjelmalla, joka ottaa huomioon 1-dimensioisen advektiivisen kulkeutumisen raossa, 1-dimensioisen diffuusion raosta kallioon, pidättymisen kallion sisäisille pinnoille sekä radioaktiivisen hajoamisen.

Tuloksia verrataan Valtion teknillisen tutkimuskeskuksen (VTT) samoille tapauksille laskemiin tuloksiin, jotka on esitetty TILA-99-turvallisuusraportissa. VTT:n käyttämä malli on sama, mutta tulokset on laskettu eri geometriassa numeerisesti.

Erot työn tulosten ja TILA-99:ssä esitettyjen tulosten välillä selittyvät suureksi osaksi vastaavien lähestymistapojen erilaisen kallioparametrien hyödyntämistavan perusteella. Työn tulokset ovat myös hyvin samankaltaisia TILA-99:n tulosten kanssa. Täten työn tulokset vahvistavat osaltaan luottamusta TILA-99:ssä esitettyihin tuloksiin.

Kallioparametrien arvojen ja veden kulkeutumisajan arvon vaihtelemisella on merkittävä vaikutus tuloksiin eräissä tapauksissa. Tulokset ovat luonnollisesti herkimpiä tapauksissa, joissa nuklidin puoliintumisaika on suhteellisen lyhyt kulkeutumisaikaan verrattuna.

# CONTENTS

ABSTRACT 3

TIIVISTELMÄ 4

CONTENTS 5

NOMENCLATURE 7

PREFACE 10

1 INTRODUCTION 11

2 PHYSICAL BACKGROUND 13
2.1 Phenomena involved 13
2.2 Flow wetted surface 13

3 HEAT TRANSFER MODEL 15
3.1 General 15
3.2 Basic equations 15
3.3 Heat transfer in a moving medium 16
3.4 Comments on the heat model 19

4 TRANSPORT MODEL 20
4.1 General 20
4.2 Retardation 20
4.3 Radioactive decay 22
4.4 Governing equation in the fracture 22
4.5 Governing equation in the matrix 23
4.6 Boundary and initial conditions 25
4.7 The transport model for a decay chain 25
4.8 1D transport model for a single nuclide 26

5 SOLUTIONS OF TRANSPORT MODELS 27
5.1 General 1D model for a single nuclide 27
5.2 1D model for a single nuclide with $D_f = 0$ 28
5.3 1D model for a single nuclide with $D_f = 0$, $\lambda = 0$ 28
5.4 The illustrative VTT model ($D_f = 0$, $\lambda = 0$) 29

6 VTT APPROACH 31
6.1 General 31
6.2 Model and data 31

7 CALCULATIONS 34
7.1 Different approaches—implications to choice of parameter values 34
7.2 Sensitivity analysis for transport resistance 34
7.3 Chosen cases 35
7.4 The calculation program 35

8 RESULTS 38
8.1 SH-sal50 and DC-ns50 scenarios 38
8.2 Sensitivity analysis 41

9 REVIEW OF THE RESULTS 42
9.1 General 42
9.2 Rock parameters 42
9.3 Rectangular approximation of the input 43
9.4 Analytical vs. numerical model—flow parameters 43
9.5 Variation of the transport resistance 44

10 DISCUSSION 45

REFERENCES 47

APPENDIX 1. Elementary Laplace transformation 48
APPENDIX 2. Derivation of the solution of 1D model with $D_f = 0$ 49
APPENDIX 3. Release rates of activation products in SH-sal50 scenario 52
APPENDIX 4. Release rates of fission products in SH-sal50 scenario 53
APPENDIX 5. Release rates of activation products in DC-ns50 scenario 54
APPENDIX 6. Release rates of fission products in DC-ns50 scenario 55
APPENDIX 7. Small release rates in SH-sal50 and DC-ns50 scenarios 56
APPENDIX 8. The calculation program 57
APPENDIX 9. The code (1/4) 58
APPENDIX 9. The code (2/4) 61
APPENDIX 9. The code (3/4) 62
APPENDIX 9. The code (4/4) 65

# NOMENCLATURE

| | |
|---|---|
| $\lambda$ | decay constant of a nuclide (1/s) |
| $\rho$ | density of water (kg/m$^3$) |
| $\kappa$ | diffusivity (m$^2$/s) |
| $\varepsilon$ | porosity of rock (–) |
| $\rho_R$ | density of solid rock (kg/m$^3$) |
| $2b$ | aperture of a fracture (m) |
| $A_B$ | surface area of a bulk volume (m$^2$) |
| $A_e$ | surface area of an elementary volume (m$^2$) |
| $a_r$ | flow wetted surface per volume of rock (m$^2$/m$^3$) |
| $a_w$ | flow wetted surface per volume of water (m$^2$/m$^3$) |
| $c$ | specific heat of medium (J/(K·kg)) |
| $C_B$ | concentration of dissolved nuclides in a bulk volume (mol/m$^3$) |
| $C_f$ | concentration of dissolved nuclides in fracture fluid (mol/m$^3$) |
| $C_p$ | concentration of dissolved nuclides in rock matrix fluid (mol/m$^3$) |
| $C_{tot}$ | total concentration of a nuclide (mol/m$^3$) |
| $D_e$ | effective diffusion coefficient from fracture to the matrix (m$^2$/s) |
| $D_f$ | hydrodynamic dispersion coefficient in fracture fluid (m$^2$/s) |
| $D_p$ | diffusion coefficient in the pore structure of rock matrix (m$^2$/s) |
| $F$ | heat flux (J/s) |
| $F_c$ | total heat flux entering a fracture element due to convection (J/s) |
| $\mathbf{f}_h$ | heat flux density vector (J/(m$^2$·s)) |
| $F_l$ | total convective heat flux leaving a fracture element to the surroundings (J/s) |
| $\mathbf{f}_{n,f}$ | nuclide flux density vector in a fracture (mol/(m$^2$·s)) |
| $\mathbf{f}_{n,p}$ | nuclide flux density vector in rock matrix (mol/(m$^2$·s)) |
| $F_{tot}$ | total time change of heat energy in a fracture element (J/s) |
| $H$ | linear heat transfer coefficient (J/(K·m$^2$·s)) |
| $K$ | thermal conductivity of medium (J/(K·m·s)) |
| $K_a$ | area based distribution coefficient (m$^3$/m$^2$) |
| $K_d$ | volume based distribution coefficient (m$^3$/kg) |
| $L$ | specific distance (m) |
| $n$ | nuclide inventory (mol) |
| $n_a$ | inventory of adsorbed and immobile nuclides (mol) |
| $n_m$ | inventory of dissolved and mobile nuclides (mol) |

| | |
|---|---|
| $n_{tot}$ | total inventory of a nuclide (mol) |
| $\dot{n}_{p,a,dec}$ | change of adsorbed nuclide inventory in a bulk volume due to radioactive decay (mol/s) |
| $\dot{n}_{f,a,dec}$ | change of adsorbed nuclide inventory in a fracture element due to radioactive decay (mol/s) |
| $\dot{n}_{f,diff}$ | diffusive loss of nuclide inventory from a fracture element at the fracture surface (mol/s) |
| $\dot{n}_{p,tot}$ | total change of nuclide inventory in a bulk volume (mol/s) |
| $\dot{n}_{f,tot}$ | total change of nuclide inventory in a fracture element (mol/s) |
| $\dot{n}_{p,m,dec}$ | change of mobile nuclide inventory in a bulk volume due to radioactive decay (mol/s) |
| $\dot{n}_{f,m,dec}$ | change of mobile nuclide inventory in a fracture element due to radioactive decay (mol/s) |
| $\dot{n}_{f,c}$ | change of nuclide inventory in a fracture element due to advection and dispersion (mol/s) |
| $\dot{n}_{p,diff}$ | diffusive change of nuclide inventory in a bulk volume (mol/s) |
| $Q$ | flow rate in a channel ($m^3/s$) |
| $q$ | Darcian velocity (m/s) |
| $\mathbf{r}$ | position vector (m) |
| $R$ | retardation coefficient (-) |
| $R_f$ | surface retardation coefficient (-) |
| $R_p$ | matrix retardation coefficient (-) |
| $R_T$ | transport resistance (s/m) |
| $S_B$ | concentration of adsorbed nuclides in a bulk volume ($mol/m^3$) |
| $S_f$ | inventory of adsorbed nuclides in a fracture per area of fracture surface ($mol/m^2$) |
| $S_p$ | inventory of adsorbed nuclides in the rock matrix per mass of rock (mol/kg) |
| $T$ | temperature (K) |
| $t$ | time (s, a) |
| $t_0$ | fixed time point (s) |
| $T_{½}$ | half life (a) |
| $T_1$ | temperature in the interior medium (K) |
| $T_2$ | temperature in the surrounding medium (K) |
| $T_s$ | surface temperature (K) |
| $t_w$ | groundwater transit time (s, a) |

| | |
|---|---|
| $u$ | parameter describing transport properties of a transport route for a species ($s^{1/2}$) |
| $W$ | width of a flow channel (m) |
| $v$ | medium velocity (m/s) |
| $\mathbf{v}$ | medium velocity vector (m/s) |
| $V_B$ | bulk volume ($m^3$) |
| $V_e$ | elementary volume ($m^3$) |
| $v_n$ | nuclide velocity (m/s) |
| $V_R$ | volume of rock in a bulk volume ($m^3$) |
| $V_W$ | volume of water in a bulk volume ($m^3$) |
| $x, y, z$ | rectangular co-ordinates (m) |

| | |
|---|---|
| $A, B, l, P, T, Y, Y', Z, ß, \eta, \gamma$ | abbreviations for various statements |
| $C^k$ | integration constants, $k$ = 1,2,… |
| $g$ | arbitrary function of position and time |
| $\mathbf{i}, \mathbf{j}, \mathbf{k}$ | unit vectors in the directions $x, y, z$, respectively |
| j | decay chain index (–) |
| k | index (–) |
| $\mathbf{n}$ | unit normal vector of an elementary volume |
| $\mathbf{n}_B$ | unit normal vector of a bulk volume |
| $p$ | Laplace variable |
| $U$ | Heaviside unit step function |
| $\alpha$ | constant |
| $\xi$ | dummy integration variable |
| $L$ | Laplace transformation operator |
| $L^{-1}$ | Laplace inverse transformation operator |
| $\overline{(\ )}$ | Laplace transform of a function |
| $\dot{(\ )}$ | time change of a function |

# PREFACE

Since 1997 as an undergraduate researcher at Radiation and Nuclear Safety Authority (STUK), I have accomplished three projects of using robust models in the safety assessment of spent fuel disposal. During these years I have gained lots of experience in this interesting and wide area of research as well as in analytical modelling. I have enjoyed doing the present work although it has also been laborious because of occurring at a time point of various changes in my life. The present work constitutes my Master's Thesis, which was approved on 7th December 1999 in the Department of Technical Physics and Mathematics in the Helsinki University of Technology (HUT).

In my work on the area of disposal I have concentrated on the phenomena occurring in the geosphere, i.e., on rock mechanics, on groundwater flow and in the present work on transport of radionuclides in the bedrock. These natural phenomena have proven to be difficult to model realistically. Especially, mathematical characterisation of the groundwater flow paths and the structure of the geosphere in general involves large uncertainties. Consequently, the models involved have to be simplified and comparison of the results to the results of other approaches is essential. One of the main principles of modelling has become familiar—a model is always only a simple image of the nature, i.e., only a possible way of describing the complex reality. Modelling has been a means of gaining experience on the area and getting better understanding on the phenomena involved.

I wish to express my gratitude to Dr.Tech. Esko Eloranta for his guidance on this and both the previous projects. The support and feedback given by him have provided me with a good background for my continuing work as a researcher.

I also thank Professor Rainer Salomaa of Helsinki University of Technology for his discussion and Lic.Phil. Risto Paltemaa of STUK for his support and advice.

Special thanks are given to Timo Vieno and Henrik Nordman of VTT for providing me with data and information fast and straightforwardly and for their favourable attitude towards the project.

Espoo, 15th March 2000 Petri Jussila

# 1 INTRODUCTION

**Background**

The objective of nuclear waste management is to permanently isolate nuclear waste from the biosphere. The Finnish approach is the final disposal of the spent fuel in crystalline bedrock. The present timetable is to select the site for the repository by the end of the year 2000. The actual disposal activities will start around the year 2020.

Radiation and Nuclear Safety Authority (STUK) is the Finnish regulator, who sets safety requirements for the final disposal of nuclear waste and verifies compliance with them. In Finland, the safety assessment and technical plans are done by the operating organisations, i.e., the implementors.

STUK's own research resources in the area of final disposal of nuclear waste are marginal and much of the proficiency for this inspection work is based on co-operation with colleagues and other experts in Finland and other countries. Student research projects, like the present study, give also insight into the problems involved in the disposal concept as well as into the verification of the research results obtained by the implementors.

**Problem**

One of the basic problems of the final disposal of nuclear waste is how to ensure isolation of the waste from biosphere for great time spans. Moving groundwater and the prevailing chemical conditions can induce degradation of the fuel disposed and transport of the released radionuclides to the biosphere via a fracture network in the geosphere. The whole field of research is complicated involving various problems that have to be taken into account, e.g., integrity of the fuel canisters, mechanical behaviour of the bentonite buffer and the rock, groundwater chemistry, thermal effects due to the heat produced by the spent fuel, characterisation of the bedrock and the flow paths of groundwater in the geosphere, transport mechanisms of groundwater in the bentonite buffer and in the geosphere, individual chemical and nuclear characteristics of each species, etc.

In this study, the problem of radionuclide transport through the geosphere is considered. The actual situation is complex, the flow paths in the geosphere are difficult to characterise and there are various phenomena involved. In a mathematical model, a critical path along which radionuclides can reach the biosphere is considered. This critical path is supposed to consist of fractures or fracture networks that are located near the repository or that possibly form in the future. The worst predictable cases and the effect of the parameters can be studied with the help of the model although it simplifies the actual situation considerably.

**Objectives**

The objectives of the present study are to gain understanding of the widely used model of radionuclide transport in porous media and to perform calculations the results of which are to be compared to those obtained by Technical Research Centre of Finland (VTT) and published in the safety assessment reports [1,2]. A Matlab® program utilising analytical models compatible with the models used by VTT is created for use of STUK.

The study is associated with a research project of STUK to utilise analytical models in safety and performance assessment for geological disposal of spent nuclear fuel. Validity and functionality of safety and performance assessments are appraised with the help of traditional analytical

models of physics and the obtained results are compared to the results of advanced and sophisticated models. The intention is to produce tools applicable to the inspection work of STUK especially for assessment of the orders of magnitudes of the results of the analyses done by the implementors.

**Scope**

In the safety assessment reports [1,2], the presented conceptual model is rather simple and analogous to a model of heat transfer from a moving medium to the surroundings. The initial step of the work was to gain understanding of the mechanisms involved in the geosphere transport and characteristics of the conceptual model. The solution of the model is given in the main reference of this study, the safety assessment report TILA-99 [1, p. 114] but the origin of the model and the derivation of the solution are not presented in the report. In a sequence of references [2, p. 145, 3] the origin is given to be found in a book by Carslaw and Jaeger [4], in which a heat transfer model analogous to particle transport is derived with a solution. However, the derivation in [4] is not straightforward and, e.g., the effect of both the walls surrounding the moving medium is not given explicitly.

An analytical solution of the actual model of radionuclide transport along a discrete fracture in a porous rock matrix, which has in the present study proven to be a generalisation of the conceptual model given in the safety assessments, was derived and published by D.H. Tang, E.O. Frind and E.A. Sudicky in 1981 [5]. However, although the solution is straightforwardly derived in the report, it does not present, e.g., the origin of the model itself and some of the parameters, e.g., the retardation coefficients. Furthermore, the derivation and the solution presented in the report do not indicate if the effects of both the fracture walls are involved.

Therefore, to understand the feasibility and characteristics of the approach used the model and the solution of it are derived in this work exhaustively.

One central parameter of geosphere transport is the transport resistance, the magnitude of which is controlled by flow rate of groundwater and the fractures of rock. Definition for the flow wetted surface included in the parameter and the influence of it in the models are controversial problems, that are to be considered in this study.

With the kind co-operation of the VTT researchers Timo Vieno and Henrik Nordman, I had the privilege to exploit the actual calculation data used in the TILA-99 report. Thereafter, actual comparative calculations for some of the results presented in TILA-99 were possible to be performed with a help of a created calculation program.

The organisation of the report is the following:

- Phenomena involved in the geosphere transport with a special attention paid to the flow wetted surface in the modelling problem are presented in Chapter 2.
- A heat transfer analogy model is derived in Chapter 3.
- Radionuclide transport models and solutions of them are derived in Chapters 4 and 5.
- The approach of VTT to perform the transport analysis and the relevant parameter data are presented in Chapter 6.
- The calculation cases with the choice of parameter values and the calculation approach are presented in Chapter 7.
- The results of the calculations are presented and reviewed in Chapters 8 and 9.
- The discussion is presented in Chapter 10.
- Derivation of the solution used in the calculations, some of the plotted results and the calculation code are presented in the Appendices.

# 2 PHYSICAL BACKGROUND

## 2.1 Phenomena involved

The transport of particles in the geosphere is closely related to the groundwater flow, which in turn is mainly affected by the bedrock characteristics and the prevailing boundary conditions. A prerequisite for the release of nuclides from the spent fuel and the subsequent transport of them to the biosphere is set by the movement of groundwater and the chemical conditions in which the corroding and dissolution of the material in a repository is possible.

The phenomena affecting the transport of radionuclides in the geosphere can be divided into advection, dispersion, retardation, and radioactive decay.

Advection describes the motion of dissolved particles along with the flowing groundwater in a single flow path.

Macroscopic flow is affected by dispersion, which is caused by, e.g., the following reasons:

- The groundwater flow is concentrated in channels, i.e., in only a part of the available fractures.
- The velocity distribution varies between the channels and within an individual channel.
- The flows in different channels meet and mix irregularly.
- Water can diffuse into the pores of solid rock matrix or in stagnant pools of the fractures.

Advection and dispersion describe basically the groundwater flow. From the point of view of particle transport, an essential additional mechanism is the retardation, which can have a significant role depending on the chemical characteristics of a particle and the groundwater. The essential meaning of retardation is that, in addition to be dissolved in groundwater, a particle can occur in a solid phase, whereupon its transport through the geosphere is delayed. Retardation occurs through sorption, which is a non-specific term for various mechanisms that bind radionuclides onto the minerals along the transport path, for example, ion exchange and surface adsorption. Sorption can occur on the surfaces of the fractures and on the inner surfaces of the rock matrix. An essential parameter affecting this mechanism is the flow wetted surface, which is considered in the following Chapter 2.2. Release rate of a single radionuclide from geosphere is reduced by the radioactive decay. If the nuclide is a member of a decay chain, the situation is significantly more complicated.

## 2.2 Flow wetted surface

This chapter is a summary of [6] discussing the role and definitions of flow wetted surface in the transport analysis. A lot of effort has been put on understanding the nature of flow paths within crystalline rock and quantifying the flow wetted surface. However, this quantification is difficult. Since the flow wetted surface is a function both of the properties of rock (fracture geometry) and of the flow field within the rock it cannot strictly be considered to be an intrinsic material property, but is dependent on flow situations and boundary conditions.

There is a trend towards considering the ratio between the flow wetted surface and the water flow rate to be a more appropriate parameter for describing the efficiency of retardation in the rock than the mere flow wetted surface. This integrated parameter has been shown to have a dominating influence on the peak release predicted from a spent fuel repository.

One definition for the flow wetted surface is the contact area between the flowing water and the fracture surfaces per unit volume of flowing water, denoted as $a_w$. This is practical in applica-

tions, where the radionuclide velocity is linearly related to the water velocity. However, for sorbing radionuclides it can be shown that the radionuclide velocity in the rock is in practice independent of the linear velocity of the water in the fractures. The nuclide velocity is then determined by the water flux or Darcian velocity $q$. In this case, it may be more convenient to use the flow wetted surface per unit volume of rock, which is denoted as $a_r$. A major problem in the definition of flow wetted surface is to properly describe the relation between the flow wetted surface and water flow rate. One alternative formulation for defining the efficiency of transfer between the water and the rock is to use the ratio of the flow wetted surface and the water flux, $a_r/q$. In the Finnish studies [1], this parameter is represented by a transport resistance $R_T$, which is essentially one half of the ratio of the flow wetted surface and the water flux. Values of these parameters, especially the local ones, are difficult to measure in practice.

Although flow occurs only in part of a fracture, the zones with more or less stagnant water can be accessed by diffusion. Thus, also the rock matrix in contact with the stagnant water can be accessible for matrix diffusion and sorption. This has been used as an argument to question the traditional way of defining the flow wetted surface. It is argued that the flow wetted surface is considerably larger than that could be deduced from the flow rate distribution. Also the accessible surface for matrix diffusion would tend to increase with time as radionuclides diffuse further into the stagnant water.

Surfaces of fractures are often rough and the fractures may also contain infillings. Thus, the actual surface area may be considerably larger than the geometrical area. However, the irregularities of the fractures usually have a very small volume and may therefore be of less importance for matrix diffusion and sorption at long time scales and for less sorbing radionuclides.

An additional problem is the persistence of flow paths, considering the long perspective that needs to be considered for transport in the geosphere. Rock stresses and thereby fracture apertures will be affected by glaciations, geochemical processes can lead to the filling of fractures, etc.

The following recommendations are given as a conclusion in [6]:

- No individual method can be selected that satisfies all requirements concerning giving relevant values, covering relevant distances and being practical to apply. Instead a combination of methods must be used.
- The long-term research should address both the detailed flow within the fractures and the effective flow wetted surface along the flow paths and its spatial variability.
- In the safety assessment modelling focus should be put on the ratio between flow wetted surface and water flux, since it has been found to be a more appropriate parameter to describe the efficiency of retardation in the rock than the flow wetted surface.
- Further development is needed of methods for assessing the flow wetted surface by evaluating the effect of interactions at the flow wetted surface.

# 3 HEAT TRANSFER MODEL

## 3.1 General

Heat transfer occurs whenever a temperature difference exists in a medium or between media. Modes of heat transfer are *conduction*, *convection* and *radiation*. *Conduction* of heat can be defined as diffusion of energy or net transfer of energy by random molecular motion, and it can occur also in a stationary medium. If a medium is in motion, an advective component of heat transfer occurs in addition. Effects of conduction and *advection* (= bulk motion of the medium) in a moving medium are together called *convection*. Thermal *radiation* occurs between surfaces of different temperature [7, p. 2–6]. When there is a solid medium between the surfaces, the effect of radiation on the total heat transfer is usually negligible.

In this study, only convection (including conduction) is taken into account in the formulation of the heat transfer problem. The problem is to calculate temperature in a moving medium and in a medium surrounding it. The governing equations are coupled by the boundary conditions at the interfaces of the media.

## 3.2 Basic equations

In an isotropic medium, conductive heat flux is assumed to occur in the direction of the negative gradient of the temperature. In addition, advective heat flux proportional to the velocity occurs if the medium is in motion. Consequently, the total heat flux density due to convection is [4, p. 13]

$$\mathbf{f}_\mathrm{h}(\mathbf{r},t) = -K(\mathbf{r})\nabla T(\mathbf{r},t) + \rho c T(\mathbf{r},t)\mathbf{v}(\mathbf{r},t), \quad (1)$$

where

$\mathbf{f}_\mathrm{h}$ is the heat flux density vector (J/(m²·s),
$\mathbf{r}$ is the position vector (m),
$t$ is time (s),
$T$ is the temperature in the medium (K)
$K$ is the thermal conductivity of the medium (J/(K·m·s)),
$\rho$ is the density of the medium (kg/m³),
$c$ is the specific heat of the medium (J/(K·kg)),
$\mathbf{v}$ is the velocity vector of the medium (m/s).

Here the density and the specific heat are assumed to be constants. In general, r and $c$ are not only functions of position, but also functions of temperature $T$, which makes the model very complicated.

When there are no heat sources or sinks in an elementary volume, the change of heat energy in it is

$$-\int_{V_\mathrm{e}} \rho c \frac{\partial T(\mathbf{r},t)}{\partial t}\, dV = \int_{A_\mathrm{e}} \mathbf{f}_\mathrm{h}(\mathbf{r},t)\cdot\mathbf{n}\, dA, \quad (2)$$

where

$V_\mathrm{e}$ is the elementary volume (m³),
$A_\mathrm{e}$ is the surface area of the elementary volume (m²),
$\mathbf{n}$ is the unit normal vector of the elementary volume.

With the help of the divergence theorem

$$\int_{A_\mathrm{e}} \mathbf{f}_\mathrm{h}(\mathbf{r},t)\cdot\mathbf{n}\, dA = \int_{V_\mathrm{e}} \nabla\cdot\mathbf{f}_\mathrm{h}(\mathbf{r},t)\, dV, \quad (3)$$

we get from (2,3) a continuity equation for an arbitrary volume

$$\rho c \frac{\partial T(\mathbf{r},t)}{\partial t} = -\nabla\cdot\mathbf{f}_\mathrm{h}(\mathbf{r},t). \quad (4)$$

From (1,4) we get *the heat equation* in moving medium

$$\frac{\partial T(\mathbf{r},t)}{\partial t} = \nabla\cdot\big(\kappa(\mathbf{r})\nabla T(\mathbf{r},t)\big) - \nabla\cdot\big(T(\mathbf{r},t)\mathbf{v}(\mathbf{r},t)\big), \qquad (5)$$

where

$$\kappa(\mathbf{r}) = \frac{K(\mathbf{r})}{\rho c} \qquad (6)$$

is the diffusivity of the medium ($m^2/s$).

## 3.3 Heat transfer in a moving medium

### General

Let us consider transfer of heat in a system consisting of medium moving in the $x$-direction with a time independent velocity $\mathbf{v} = v(x)\mathbf{i}$ between two stationary and identical semi-infinite media. The geometry of the problem is depicted in Figure 1, which applies also to the transport problem presented in Chapter 4. The variables of the problem are the following:

- $T_1(x,t)$ is the temperature in the interior medium, $|z| < b$,
- $T_2(\mathbf{r},t)$ is the temperature in the surrounding media, $|z| > b$.

There is a steady heat source of constant temperature $T_0$ at $x = y = 0$. The thickness $2b$ of the interior medium is very small and the temperature in it is not assumed to depend on the $z$-co-ordinate (and $y$-co-ordinate). This refers to perfect heat conductivity of solid medium or to perfectly stirred fluid. Heat is transferred by convection in the interior medium and by conduction in the surrounding medium.

The governing equations are obtained by deriving a heat balance equation for an element in the interior depicted in Figure 2 with the help of the basic equations of Chapter 3.2. Figure 2 applies also to the transport problem presented in Chapter 4.

### Convection in the interior medium

The change of heat energy in the element is due to convection in the $x$-direction and convection heat transfer to the surrounding medium in the $z$-direction. Because time is not explicitly involved in equations (7–9), we denote $T(x,t) = T(x)$ for brevity. The heat flux entering the element through its vertical surface at $x$ is by (1)

$$F(x) = -2b\Delta y K_1(x)\frac{\partial T_1(x)}{\partial x} + 2b\Delta y \rho_1 c_1 T_1(x) v(x), \qquad (7)$$

where

$F(x)$ is the entering heat flux due to convection at $x$ (J/s),

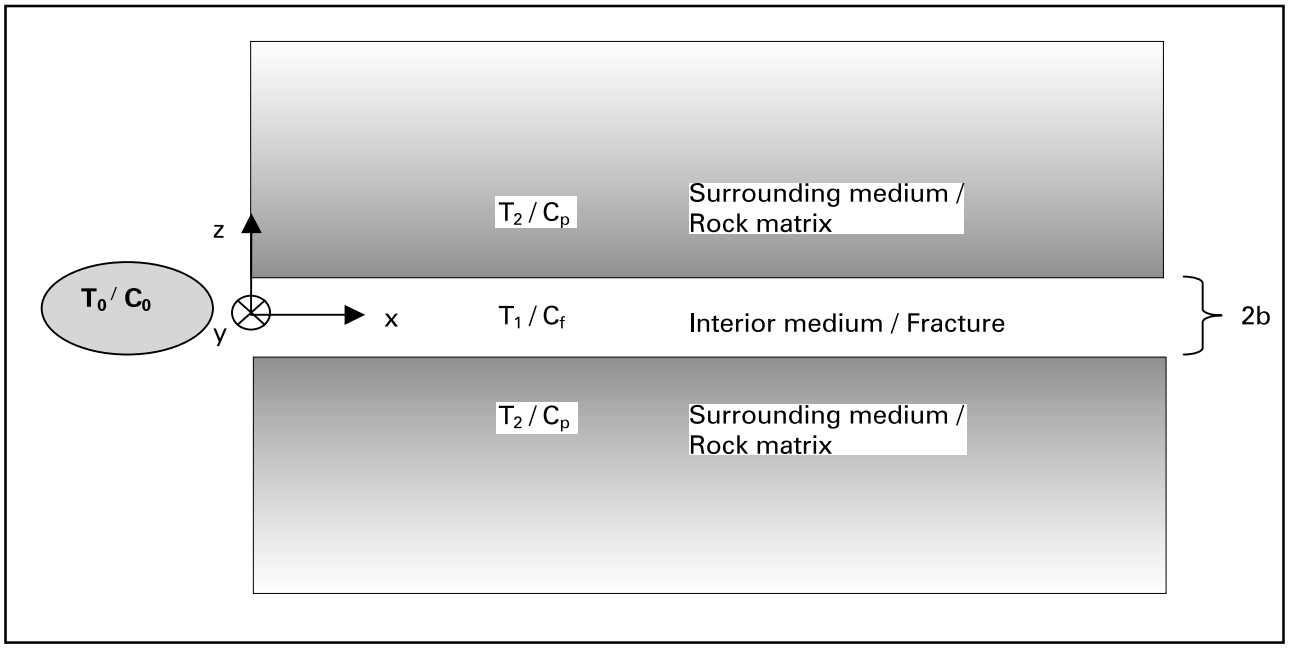


***Figure 1.*** *The geometry of the heat problem (Chapter 3) / transport problem (Chapter 4).*

$K_1$ is the thermal conductivity of the interior medium (J/(K·m·s)),
$\rho_1$ is the density of the interior medium (kg/m$^3$),
$c_1$ is the specific heat of the interior medium (J/(K·kg)).

The total heat flux entering the element through its vertical surface at $x+dx$ is

$$
\begin{aligned}
&F(x+dx) = \\
&2b\Delta y K_1(x+dx)\frac{\partial T_1(x+dx)}{\partial x} - 2b\Delta y \rho_1 c_1 T_1(x+dx)v(x+dx) \\
&= 2b\Delta y\left( K_1(x) + \frac{\partial K_1(x)}{\partial x}dx + \ldots \right)\frac{\partial}{\partial x}\left( T_1(x) + \frac{\partial T_1(x)}{\partial x}dx + \ldots \right) - \\
&-2b\Delta y \rho_1 c_1\left( T_1(x) + \frac{\partial T_1(x)}{\partial x}dx + \ldots \right)\left( v(x) + \frac{\partial v(x)}{\partial x}dx + \ldots \right) \\
&\approx 2b\Delta y\left( K_1(x)\frac{\partial T_1(x)}{\partial x} + K_1(x)\frac{\partial^2 T_1(x)}{\partial x^2}dx + \frac{\partial K_1(x)}{\partial x}\frac{\partial T_1(x)}{\partial x}dx + \frac{\partial K_1(x)}{\partial x}\frac{\partial^2 T_1(x)}{\partial x^2}(dx)^2 \right) - \\
&-2b\Delta y \rho_1 c_1\left( T_1(x)v(x) + T_1(x)\frac{\partial v(x)}{\partial x}dx + \frac{\partial T_1(x)}{\partial x}v(x)dx + \frac{\partial T_1(x)}{\partial x}\frac{\partial v(x)}{\partial x}(dx)^2 \right) \quad ,
\end{aligned}
\tag{8}
$$

where
$F(x+dx)$ is the entering heat flux due to convection at $x+dx$ (J/s).

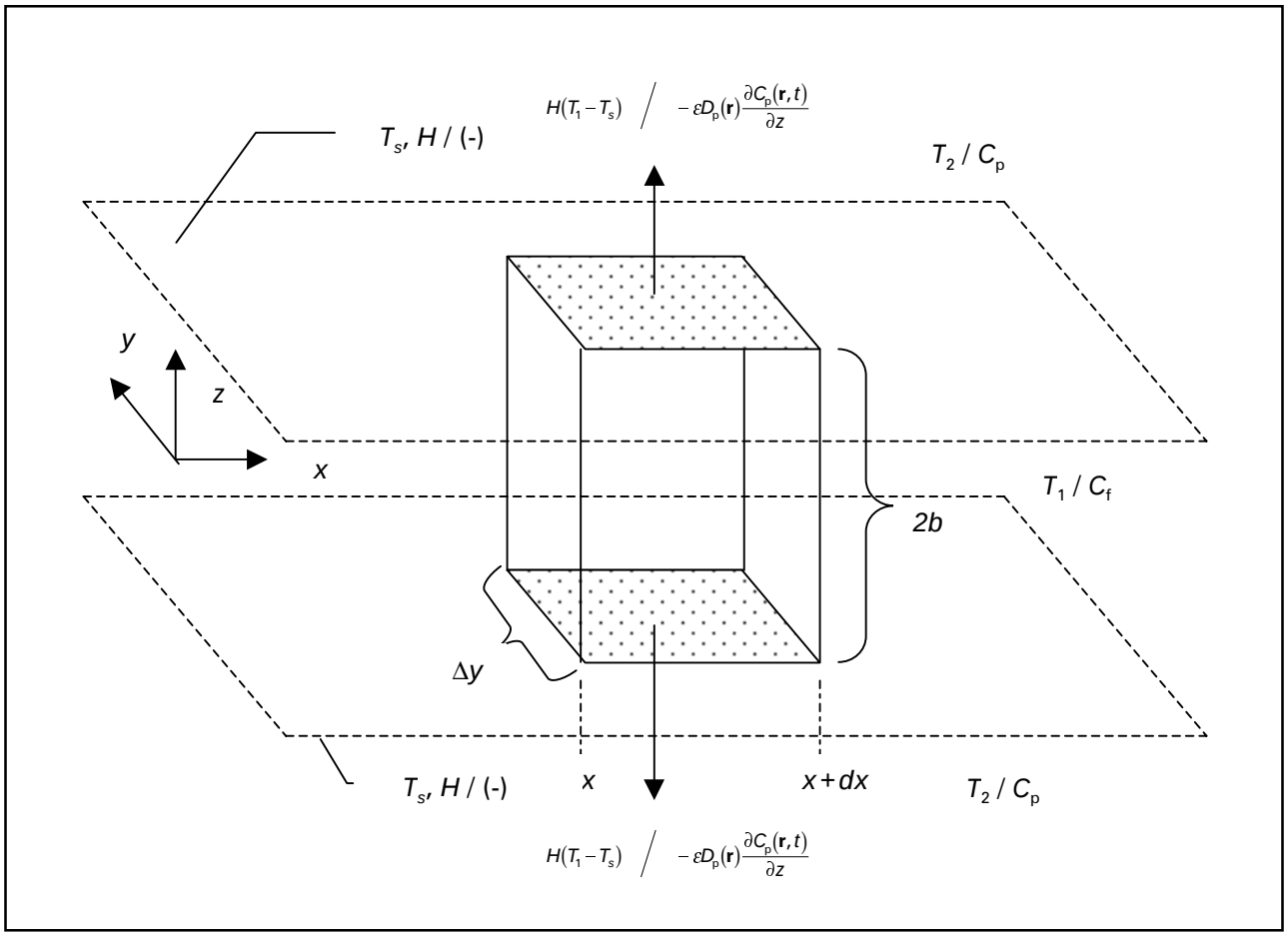


***Figure 2.*** *An element in the interior medium in the heat problem (Chapter 3) / a fracture element in the transport problem (Chapter 4).*

In (8), we have used the *Taylor approximation*. By equating the double differentials $(dx)^2$ in (8) to zero and summing (7) and (8) we get to the first order in $dx$ the total heat flux entering the element in $x$-direction due to convection to be

$$\begin{aligned} F_c &= F(x) + F(x+dx) \approx \\ &\approx 2b\Delta y\left( K_1(x)\frac{\partial^2 T_1(x)}{\partial x^2} + \frac{\partial K_1(x)}{\partial x}\frac{\partial T_1(x)}{\partial x}\right)dx - \\ &-2b\Delta y\rho_1 c_1\left( T_1(x)\frac{\partial v(x)}{\partial x} + \frac{\partial T_1(x)}{\partial x}v(x)\right)dx \\ &= 2b\Delta y\frac{\partial}{\partial x}\left( K_1(x)\frac{\partial T_1(x)}{\partial x}\right)dx \\ &-2b\Delta y\rho_1 c_1\frac{\partial}{\partial x}\big(v(x)T_1(x)\big)dx \quad , \end{aligned} \tag{9}$$

where

$F_c$ is the total heat flux entering the element due to convection (J/s).

**Convection heat transfer to the surrounding medium**

The total loss of heat energy in $z$-direction from the interior medium to the surrounding medium through the two horizontal surfaces at $z = \pm b$ in unit time is by *Newton's law of cooling* [7, p. 8, 245]

$$F_l = -2H\big(T_1(x,t) - T_s(x,t)\big)\Delta y dx, \tag{10}$$

where

$F_l$ is the total convective heat flux leaving the element and entering the surrounding medium (J/s),

$H$ is the convection heat transfer coefficient (J/(K·m²·s)),

$T_s$ is the surface temperature at the boundaries of the media (K).

In (10), the situation is assumed to be symmetric in relation to the $xy$-plane. The surrounding media are identical, the interior medium is moving in the $x$-direction only and the temperature in the interior medium is constant in the $z$-direction. Consequently, the convective losses out of the element through the two horizontal surfaces at $z = \pm b$ are equal and the total loss is twice the loss through each of the surfaces.

**Total change of heat energy in the interior medium**

The total time change of heat energy in the element is

$$F_{tot} = \frac{\partial}{\partial t}\big(2b\Delta y\rho_1 c_1 T_1(x,t)dx\big) = 2b\Delta y\rho_1 c_1\frac{\partial T_1(x,t)}{\partial t}dx, \tag{11}$$

where

$F_{tot}$ is the total time change of heat energy in the element (J/s).

**The governing equation in the interior medium**

The heat balance equation in the element is obtained from (9–11) to be

$$\begin{aligned} &F_{tot} = F_c + F_l \\ &\Leftrightarrow \\ &2b\Delta y\rho_1 c_1\frac{\partial T_1(x,t)}{\partial t}dx = \\ &2b\Delta y\frac{\partial}{\partial x}\left( K_1(x)\frac{\partial T_1(x,t)}{\partial x}\right)dx \\ &-2b\Delta y\rho_1 c_1\frac{\partial}{\partial x}\big(v(x)T_1(x,t)\big)dx - \\ &-2H\big(T_1(x,t) - T_s(x,t)\big)\Delta y dx, \end{aligned} \tag{12}$$

and from (6,12) we get

$$\begin{aligned} \frac{\partial T_1(x,t)}{\partial t} &= \frac{\partial}{\partial x}\left(\kappa_1(x)\frac{\partial T_1(x,t)}{\partial x}\right) - \frac{\partial}{\partial x}\big(v(x)T_1(x,t)\big) \\ &-\frac{2}{2b}\frac{H}{\rho_1 c_1}\big(T_1(x,t) - T_s(x,t)\big), \end{aligned} \tag{13}$$

where

$\kappa_1$ is the diffusivity of the interior medium (m²/s).

The boundary conditions at $z = \pm b$ are of the type [7, p. 51]

$$\left(-K_2(\mathbf{r})\frac{\partial T_2(\mathbf{r},t)}{\partial z}\right)_{|z=\pm b} = H\big(T_1(x,t) - T_s(x,t)\big), \tag{14}$$

where

$K_1$ is the thermal conductivity of the surrounding medium (J/(K·m·s)).

By substituting the boundary condition (14) to (13) we get

$$\frac{\partial T_1(x,t)}{\partial t} = \frac{\partial}{\partial x}\left(\kappa_1(x)\frac{\partial T_1(x,t)}{\partial x}\right) - \frac{\partial}{\partial x}\left(v(x)T_1(x,t)\right) + \\ + \frac{2}{2b}\left(\frac{K_2(\mathbf{r})}{\rho_1 c_1}\frac{\partial T_2(\mathbf{r},t)}{\partial z}\right)\Bigg|_{|z|=b}; \quad |z| = b, \tag{15}$$

which is the governing equation in the interior medium.

**The governing equation in the surrounding medium**

The governing equation for the surrounding medium is readily obtained from (5) for the stationary medium (**v** = **0**):

$$\frac{\partial T_2(\mathbf{r},t)}{\partial t} = \nabla\cdot\left(\kappa_2(\mathbf{r})\nabla T_2(\mathbf{r},t)\right); \quad |z| \geq b, \tag{16}$$

where

$\kappa_2$ is the diffusivity of the surrounding medium ($m^2/s$).

**Boundary and initial conditions**

An additional condition for the problem is the continuity of the temperature at the boundaries

$$T_1(x,t) = T_2(\mathbf{r},t); \quad |z| = b. \tag{17}$$

With a condition at the inlet of the fracture ($x = 0$) and an initial condition

$$T_1(x=0,t) = T_0, \\ T_2(\mathbf{r}, t=0) = 0, \tag{18}$$

the heat transfer problem (15–18) is completely defined.

## 3.4 Comments on the heat model

The continuity condition at the boundary (17) conflicts with the definition of the convective heat transfer assumed earlier in the model derivation (10) in which the transfer is assumed to occur if there is a temperature difference between the interior medium and the boundary. In [4, p. 396], the situation is simply passed by stating that the situation refers to very large $H$ in the model.

To be exact, since the unit of temperature has been determined to be K, the latter of the initial conditions in (18) is unphysical, because it assumes an absolute zero temperature. However, this is not a practical problem, since the unit can be arbitrarily selected.

# 4 TRANSPORT MODEL

## 4.1 General

The heat transfer model derived above has a transport model analogy, in which temperature (K) is replaced by concentration of nuclides (mol/m$^3$) dissolved in water. The geometry is the same as in the heat transfer problem (Figure 1). A fracture full of water represents the interior medium and the surrounding medium is a rock matrix consisting of solid rock with a pore structure full of diffused water. The choice of the inlet condition does not affect the derivation of the model, as it did not in the derivation of the heat problem, either. An analytical solution can be found at least for an inlet condition of a constant source of nuclides, which will be used in the solution phase in Chapter 5.

A general 1D transport model for a single nuclide is presented in a paper by Tang, Frind and Sudicky [5] and it can be generalised further to account for decay chains of nuclides. In the present chapter, the general model is derived with a help of parameter definitions given in a VTT report [8].

The following processes are to be considered [5, p. 555]:

- advective transport along the fracture,
- mechanical dispersion in the fracture,
- diffusion within the fracture, in the direction of the fracture axis,
- diffusion from the fracture into and within the matrix,
- adsorption on the fracture surfaces,
- adsorption within the matrix and
- radioactive decay.

Longitudinal mechanical dispersion describes the combined effects of mixing in the direction of the fracture axis due to the parabolic velocity profile and the roughness of the fracture walls.

In the definition of heat flux density (1), the coefficient $K$ describes (only) the effect of thermal conduction of (or diffusion of heat in) the medium. The equivalent coefficient ($D_f$) in the transport problem includes the effects of dispersion along the fracture axis and molecular diffusion in water, which mechanisms are defined under the term *hydrodynamic dispersion*.

In the heat transfer problem, we had only two variables (see Chapter 3.3). Because of the retardation mechanisms, we have four variables in the transport problem:

1. $C_f$ is the concentration of dissolved and mobile nuclides in fracture fluid (mol/m$^3$),
2. $S_f$ is the inventory of adsorbed and immobile nuclides in fracture per area of fracture surface (mol/m$^2$),
3. $C_p$ is the concentration of dissolved and mobile nuclides in the rock matrix fluid (mol/m$^3$),
4. $S_p$ is the inventory of adsorbed and immobile nuclides in the rock matrix per mass of rock (mol/kg).

In the transport model, nuclides can either be dissolved in water and mobile or adsorbed to a solid phase and immobile. The number of the variables can be reduced to two also in the transport problem by using a modelling tool called a *linear equilibrium isotherm*, according to which the ratio of adsorbed nuclide inventory and the dissolved inventory is defined as a distribution coefficient.

## 4.2 Retardation

Retardation can occur due to adsorption to the fracture surfaces or to the inner surfaces of the pore structure of the rock matrix. An area based distribution coefficient is defined as [8, p. 30]

$$K_a = \frac{S_f}{C_f}, \quad (19)$$

where

$K_a$ is the area based distribution coefficient ($m^3/m^2$),

while a volume based distribution coefficient is defined as [8, p. 29]

$$K_d = \frac{S_p}{C_p}, \quad (20)$$

where

$K_d$ is the volume based distribution coefficient ($m^3/kg$).

In [8, p. 35], the inverse of a retardation coefficient is defined as the mobile fraction of the nuclide inventory. A definition for any retardation coefficient can thus be

$$R = \frac{n_{tot}}{n_m} = \frac{n_m + n_a}{n_m} = 1 + \frac{n_a}{n_m}, \quad (21)$$

where

$R$ is a retardation coefficient (–),

$n_{tot}$ is the total nuclide inventory (mol),

$n_m$ is the fraction of the nuclide inventory that is dissolved in water and considered mobile (mol),

$n_a$ is the adsorbed and immobile fraction of the nuclide inventory (mol).

In the fracture, nuclides can be dissolved in water or adsorbed on the fracture surfaces. In the element in Figure 2, the area based distribution coefficient in the fracture (19) takes the form

$$K_a = \frac{n_a/(2\Delta y dx)}{n_m/(2b\Delta y dx)} = \frac{2b}{2}\frac{n_a}{n_m}. \quad (22)$$

From (21,22) we get a statement for the retardation coefficient in the fracture to be

$$R = R_f = 1 + \frac{2}{2b}K_a, \quad (23)$$

where we have a definition:

$R_f$ is the surface retardation coefficient in the fracture (–).

Here the factor $2/2b$ represents the flow wetted surface per water volume in the fracture, which is equivalent to $a_w$ as defined in Chapter 2.2.

The surface retardation coefficient expresses also the ratio of the water velocity to the nuclide velocity [8, p. 35]

$$R_f = \frac{v}{v_n}, \quad (24)$$

where

$v_n$ is the nuclide velocity (m/s).

In the rock matrix, nuclides can either be dissolved in water diffused in the pore structure of the rock or adsorbed in the inner surfaces of the pores. A bulk volume in the pore structure (Figure 3) consists of water and rock, i.e.,

$$V_B = V_W + V_R, \quad V_R = (1-\varepsilon)V_B, \quad V_W = \varepsilon V_B, \quad (25)$$

where

$V_B$ is the bulk volume ($m^3$),

$V_W$ is the volume of water in the bulk volume ($m^3$),

$V_R$ is the volume of rock in the bulk volume ($m^3$),

$\varepsilon$ is the porosity of the rock (–).

The definition of the porosity in (25) assumes that the whole pore structure is full of water. From (20,25), the volume based distribution coefficient in the rock matrix takes the form

$$K_d = \frac{n_a/(\rho_R V_R)}{n_m/V_W} = \frac{n_a/(\rho_R(1-\varepsilon)V_B)}{n_m/\varepsilon V_B} = \frac{\varepsilon}{\rho_R(1-\varepsilon)}\frac{n_a}{n_m}, \quad (26)$$

where

$\rho_R$ is the density of solid rock ($kg/m^3$).

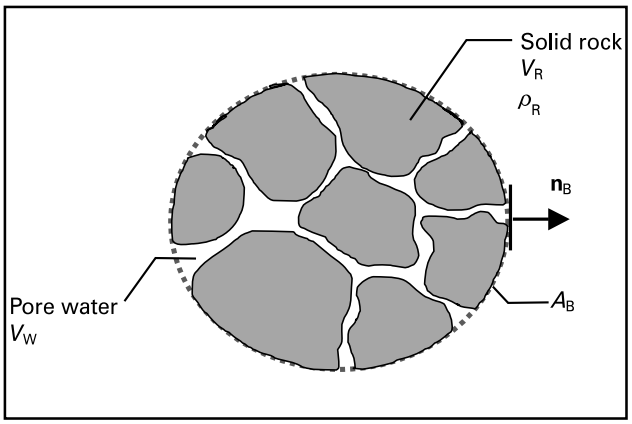


***Figure 3.*** *Bulk volume $V_B$ of the rock matrix.*

From (21,26) we get a statement for the retardation coefficient in the rock matrix to be

$$R = R_{\mathrm{p}} = 1 + \frac{\rho_{\mathrm{R}}(1-\varepsilon)}{\varepsilon} K_{\mathrm{d}}, \tag{27}$$

where we have a definition:
$R_{\mathrm{p}}$ is the matrix retardation coefficient (–).

The statements for the retardation coefficients (23,27) have also been derived by K. Rasilainen in [9].

## 4.3 Radioactive decay

The rate of change of amount (inventory or concentration) of a nuclide due to radioactive decay is directly proportional to its amount

$$\frac{\partial C}{\partial t} = -\lambda C, \tag{28}$$

where
$\lambda$ is the decay constant of a nuclide (1/s).

When multiple radionuclides are involved, the descending decay chain 1, ..., j–1, j, j+1, ... of the nuclides has to be taken into account in the inventory calculations. E.g., when there is only one mother nuclide $C_{\mathrm{j-1}}$ in the nuclide chain, the rate of change of the j$^{\mathrm{th}}$ nuclide $C_{\mathrm{j}}$ is

$$\frac{\partial C_{\mathrm{j}}}{\partial t} = \lambda_{\mathrm{j-1}} C_{\mathrm{j-1}} - \lambda_{\mathrm{j}} C_{\mathrm{j}}. \tag{29}$$

## 4.4 Governing equation in the fracture

**Advection and dispersion in fracture fluid**

The situation is the same as in the heat transfer problem. The geometry of the problem is as in Figure 1 and the governing equation in fracture is obtained by deriving the balance equation in a fracture element (Figure 2). The flux density of nuclides dissolved in moving fracture fluid analogous to the heat flux density in (1) is

$$\mathbf{f}_{n,\mathrm{f}}(\mathbf{r},t) = -D_{\mathrm{f}}(\mathbf{r})\nabla C_{\mathrm{f}}(\mathbf{r},t) + C_{\mathrm{f}}(\mathbf{r},t)\mathbf{v}(\mathbf{r},t), \tag{30}$$

where
$\mathbf{f}_{n,\mathrm{f}}$ is the nuclide flux density vector in fracture (mol/(m$^2$·s)),

$D_{\mathrm{f}}$ is the hydrodynamic dispersion coefficient (m$^2$/s),
$\mathbf{v}$ is the water velocity vector (m/s).

In analogy to (9), the change of nuclide inventory in the element in Figure 2 is due to advection and dispersion

$$\dot{n}_{\mathrm{f,c}} \approx 2b\Delta y \frac{\partial}{\partial x}\left( D_{\mathrm{f}}(x)\frac{\partial C_{\mathrm{f}}(x,t)}{\partial x}\right)dx - 2b\Delta y \frac{\partial}{\partial x}\left(v(x)C_{\mathrm{f}}(x,t)\right)dx, \tag{31}$$

where
$\dot{n}_{\mathrm{f,c}}$ is the change of nuclide inventory in the element due to advection and dispersion (mol/s).

**Diffusion out of fracture fluid**

Analogous to the convective heat flux $F_{\mathrm{l}}$ (10,14) is the diffusive loss of nuclides from the element to the pores of the fracture surface, which by *Fick's first law* is

$$\dot{n}_{\mathrm{f,diff}} = 2\left( \varepsilon D_{\mathrm{p}}(\mathbf{r})\frac{\partial C_{\mathrm{p}}(\mathbf{r},t)}{\partial z}\right)\Big|_{|z|=b} \Delta y dx, \tag{32}$$

where
$\dot{n}_{\mathrm{f,diff}}$ is the diffusive loss of nuclide inventory from the element at the fracture surfaces (mol/s),

$D_{\mathrm{p}}$ is the diffusion coefficient in the pore structure of rock matrix (m$^2$/s).

The coefficient 2 in (32) is due to diffusive loss to both the fracture surfaces and due to the symmetry of the situation. The occurrence of porosity $\varepsilon$ in (32) indicates, that only a fraction of the surface area is available for the diffusion to occur, a situation of which is different from that of the convective loss of heat (10,14).

**Change due to radioactive decay**

The change of mobile nuclide inventory in the element due to radioactive decay is from (28)

$$\dot{n}_{\mathrm{f,m,dec}} = -\lambda C_{\mathrm{f}}(x,t)2b\Delta y dx, \tag{33}$$

where

$\dot{n}_{\mathrm{f,m,dec}}$ is the change of mobile nuclide inventory in the element due to radioactive decay (mol/s).

Similarly, the change of nuclide inventory adsorbed in the element due to radioactive decay is

$$\dot{n}_{\mathrm{f,a,dec}} = -2\lambda S_{\mathrm{f}}(x,t)\Delta y dx, \tag{34}$$

where

$\dot{n}_{\mathrm{f,a,dec}}$ is the change of adsorbed nuclide inventory in the element due to radioactive decay (mol/s).

**Total change in the fracture fluid**

The total change of nuclide inventory in the element is

$$\begin{aligned}\dot{n}_{\mathrm{f,tot}} &= \frac{\partial}{\partial t}\left(2b\Delta y C_{\mathrm{f}}(x,t)dx + 2S_{\mathrm{f}}(x,t)\Delta y dx\right)\\ &= 2b\Delta y\frac{\partial C_{\mathrm{f}}(x,t)}{\partial t}dx + 2\Delta y\frac{\partial S_{\mathrm{f}}(x,t)}{\partial t}dx \quad ,\end{aligned} \tag{35}$$

where

$\dot{n}_{\mathrm{f,tot}}$ is the total change of nuclide inventory in the element (mol/s).

**The governing equation in the fracture**

The total change of nuclide inventory in the element is obtained from (31–35) to be

$$\begin{aligned}&\dot{n}_{\mathrm{f,tot}} = \dot{n}_{\mathrm{f,c}} + \dot{n}_{\mathrm{f,m,dec}} + \dot{n}_{\mathrm{f,a,dec}} + \dot{n}_{\mathrm{f,diff}}\\ &\Leftrightarrow\\ &2b\Delta y\frac{\partial C_{\mathrm{f}}(x,t)}{\partial t}dx + 2\Delta y\frac{\partial S_{\mathrm{f}}(x,t)}{\partial t}dx =\\ &2b\Delta y\frac{\partial}{\partial x}\left(D_{\mathrm{f}}(x)\frac{\partial C_{\mathrm{f}}(x,t)}{\partial x}\right)dx\\ &-2b\Delta y\frac{\partial}{\partial x}\left(v(x)C_{\mathrm{f}}(x,t)\right)dx -\\ &-2b\Delta y\lambda C_{\mathrm{f}}(x,t)dx - 2\Delta y\lambda S_{\mathrm{f}}(x,t)dx\\ &+2\Delta y\left(\varepsilon D_{\mathrm{p}}(\mathbf{r})\frac{\partial C_{\mathrm{p}}(\mathbf{r},t)}{\partial z}\right)\Bigg|_{|z|=b}dx \quad ,\end{aligned} \tag{36}$$

from which we can get the form

$$\begin{aligned}&\frac{\partial C_{\mathrm{f}}(x,t)}{\partial t} + \frac{2}{2b}\frac{\partial S_{\mathrm{f}}(x,t)}{\partial t}\\ &= \frac{\partial}{\partial x}\left(D_{\mathrm{f}}(x)\frac{\partial C_{\mathrm{f}}(x,t)}{\partial x}\right) - \frac{\partial}{\partial x}\left(v(x)C_{\mathrm{f}}(x,t)\right) -\\ &-\lambda C_{\mathrm{f}}(x,t) - \frac{2}{2b}\lambda S_{\mathrm{f}}(x,t) + \frac{2}{2b}\left(\varepsilon D_{\mathrm{p}}(\mathbf{r})\frac{\partial C_{\mathrm{p}}(\mathbf{r},t)}{\partial z}\right)\Bigg|_{|z|=b}.\end{aligned} \tag{37}$$

By introducing *a linear equilibrium isotherm* the adsorbed nuclide inventory is assumed to be directly proportional to the nuclide inventory in fluid, see (19):

$$S_{\mathrm{f}} = K_{\mathrm{a}}C_{\mathrm{f}}, \tag{38}$$

$$\frac{\partial S_{\mathrm{f}}}{\partial t} = K_{\mathrm{a}}\frac{\partial C_{\mathrm{f}}}{\partial t}. \tag{39}$$

By substituting (38,39) to (37) we get

$$\begin{aligned}&\left(1+\frac{2}{2b}K_{\mathrm{a}}\right)\frac{\partial C_{\mathrm{f}}(x,t)}{\partial t} =\\ &\frac{\partial}{\partial x}\left(D_{\mathrm{f}}(x)\frac{\partial C_{\mathrm{f}}(x,t)}{\partial x}\right) - \frac{\partial}{\partial x}\left(v(x)C_{\mathrm{f}}(x,t)\right)\\ &-\lambda\left(1+\frac{2}{2b}K_{\mathrm{a}}\right)C_{\mathrm{f}}(x,t) + \frac{2}{2b}\left(\varepsilon D_{\mathrm{p}}(\mathbf{r})\frac{\partial C_{\mathrm{p}}(\mathbf{r},t)}{\partial z}\right)\Bigg|_{|z|=b},\end{aligned} \tag{40}$$

and with the definition (23) of the surface retardation coefficient, (40) becomes

$$\begin{aligned}&\frac{\partial C_{\mathrm{f}}(x,t)}{\partial t} = \frac{\partial}{\partial x}\left(\frac{D_{\mathrm{f}}(x)}{R_{\mathrm{f}}}\frac{\partial C_{\mathrm{f}}(x,t)}{\partial x}\right)\\ &-\frac{\partial}{\partial x}\left(\frac{v(x)}{R_{\mathrm{f}}}C_{\mathrm{f}}(x,t)\right) -\\ &-\lambda C_{\mathrm{f}}(x,t) + \frac{2}{2b}\left(\frac{\varepsilon D_{\mathrm{p}}(\mathbf{r})}{R_{\mathrm{f}}}\frac{\partial C_{\mathrm{p}}(\mathbf{r},t)}{\partial z}\right)\Bigg|_{|z|=b}; |z| = b,\end{aligned} \tag{41}$$

which is the governing equation in the fracture.

## 4.5 Governing equation in the matrix

**Inventories in the matrix**

In the matrix, nuclides can be dissolved in the matrix fluid or adsorbed to the inner surfaces of the pore structure. As in the case of fracture fluid,

in which the governing equation was derived from the balance in a fracture element, we use the balance in a bulk volume $V_B$ (Figure 3) to derive the governing equation for the matrix.

With the help of definition of the concentration in the matrix fluid $C_p$ (see Chapter 4.1) and the definition of the bulk volume (25), we can derive the concentration of dissolved nuclides in the bulk volume around **r** to be

$$C_B(\mathbf{r},t) = \frac{n_m(\mathbf{r},t)}{V_B} = \frac{n_m(\mathbf{r},t)}{V_w/\varepsilon} = \varepsilon C_p(\mathbf{r},t), \tag{42}$$

where

$C_B$ is the concentration of dissolved and mobile nuclides in the bulk volume (mol/m$^3$).

With the help of the definition of the adsorbed nuclide inventory per mass of solid $S_p$ (20) and the definition of the bulk volume (25), we can derive the concentration of adsorbed nuclides in the bulk volume around **r** to be

$$\begin{aligned} S_B(\mathbf{r},t) &= \frac{n_a(\mathbf{r},t)}{V_B} = \frac{n_a(\mathbf{r},t)}{V_R/(1-\varepsilon)} = \rho_R(1-\varepsilon)\frac{n_a(\mathbf{r},t)}{\rho_R V_R} \\ &= \rho_R(1-\varepsilon)S_p(\mathbf{r},t), \end{aligned} \tag{43}$$

where

$S_B$ is the concentration of adsorbed and immobile nuclides in the bulk volume (mol/m$^3$).

**Diffusion in the matrix**

The diffusive flux density of nuclides dissolved in fluid in stationary rock matrix is

$$\mathbf{f}_{n,p}(\mathbf{r},t) = -\varepsilon D_p(\mathbf{r})\nabla C_p(\mathbf{r},t), \tag{44}$$

where

$\mathbf{f}_{n,p}$ is the nuclide flux density vector in the matrix (mol/(m$^2$·s)).

With the help of *the divergence theorem* (3) and (44), the change of nuclide inventory in a bulk volume due to diffusion is

$$\begin{aligned} \dot{n}_{p,diff} &= -\int_{A_B} \mathbf{f}_{n,p}\cdot\mathbf{n}_B\,dA \\ &= -\int_{V_B} \nabla\cdot\mathbf{f}_{n,p}\,dV = \int_{V_B} \nabla\cdot\left(\varepsilon D_p(\mathbf{r})\nabla C_p(\mathbf{r},t)\right)dV, \end{aligned} \tag{45}$$

where

$\dot{n}_{p,diff}$ is the diffusive change of the nuclide inventory in the bulk volume (mol/s),

$A_B$ is the area of the surface of the bulk volume (m$^2$),

$\mathbf{n}_B$ is a unit normal vector of the bulk volume.

**Change due to radioactive decay**

The change of dissolved and mobile nuclide inventory in the bulk volume due to radioactive decay is from (28,42)

$$\dot{n}_{p,m,dec} = -\int_{V_B} \lambda C_B(\mathbf{r},t)\,dV = -\int_{V_B} \lambda\varepsilon C_p(\mathbf{r},t)\,dV, \tag{46}$$

where

$\dot{n}_{p,m,dec}$ is the change of mobile nuclide inventory in the bulk volume due to radioactive decay (mol/s).

Similarly, the change of adsorbed and immobile nuclide inventory in the bulk volume due to radioactive decay is from (28,43)

$$\dot{n}_{p,a,dec} = -\int_{V_B} \lambda S_B(\mathbf{r},t)\,dV = -\int_{V_B} \lambda\rho_R(1-\varepsilon)S_p(\mathbf{r},t)\,dV,$$

where (47)

$\dot{n}_{p,a,dec}$ is the change of adsorbed nuclide inventory in the bulk volume due to radioactive decay (mol/s).

**Total change in the bulk volume**

The total change of nuclide inventory in the bulk volume is from (42,43)

$$\begin{aligned} \dot{n}_{p,tot} &= \int_{V_B} \frac{\partial}{\partial t}\left(C_B(\mathbf{r},t) + S_B(\mathbf{r},t)\right)dV \\ &= \int_{V_B} \left(\varepsilon\frac{\partial C_p(\mathbf{r},t)}{\partial t} + \rho_R(1-\varepsilon)\frac{\partial S_p(\mathbf{r},t)}{\partial t}\right)dV, \end{aligned} \tag{48}$$

where

$\dot{n}_{p,tot}$ is the total change of nuclide inventory in the bulk volume (mol/s).

**The governing equation in the rock matrix**

The total change of nuclide inventory in the bulk volume is obtained from (45–48) to be

$$\dot{n}_{\mathrm{p,tot}} = \dot{n}_{\mathrm{p,diff}} + \dot{n}_{\mathrm{p,m,dec}} + \dot{n}_{\mathrm{p,a,dec}}$$

$$\Leftrightarrow$$

$$\int_{V_B}\left(\varepsilon\frac{\partial C_{\mathrm{p}}(\mathbf{r},t)}{\partial t} + \rho_{\mathrm{R}}(1-\varepsilon)\frac{\partial S_{\mathrm{p}}(\mathbf{r},t)}{\partial t}\right)dV =$$

$$\int_{V_B}\nabla\cdot\left(\varepsilon D_{\mathrm{p}}(\mathbf{r})\nabla C_{\mathrm{p}}(\mathbf{r},t)\right)dV - \int_{V_B}\lambda\varepsilon C_{\mathrm{p}}(\mathbf{r},t)dV \qquad (49)$$

$$-\int_{V_B}\lambda\rho_{\mathrm{R}}(1-\varepsilon)S_{\mathrm{p}}(\mathbf{r},t)dV.$$

With an arbitrary bulk volume and by dividing by $\varepsilon$ we get from (49)

$$\frac{\partial C_{\mathrm{p}}(\mathbf{r},t)}{\partial t} + \rho_{\mathrm{R}}\frac{(1-\varepsilon)}{\varepsilon}\frac{\partial S_{\mathrm{p}}(\mathbf{r},t)}{\partial t} = \qquad (50)$$

$$\nabla\cdot\left(D_{\mathrm{p}}(\mathbf{r})\nabla C_{\mathrm{p}}(\mathbf{r},t)\right) - \lambda C_{\mathrm{p}}(\mathbf{r},t) - \lambda\rho_{\mathrm{R}}\frac{(1-\varepsilon)}{\varepsilon}S_{\mathrm{p}}(\mathbf{r},t).$$

By defining another *linear equilibrium isotherm* of the form (see (20))

$$S_{\mathrm{p}} = K_{\mathrm{d}}C_{\mathrm{p}}, \qquad (51)$$

$$\frac{\partial S_{\mathrm{p}}}{\partial t} = K_{\mathrm{d}}\frac{\partial C_{\mathrm{p}}}{\partial t}, \qquad (52)$$

we get from (50–52)

$$\left(1+\rho_{\mathrm{R}}\frac{(1-\varepsilon)}{\varepsilon}K_{\mathrm{d}}\right)\frac{\partial C_{\mathrm{p}}(\mathbf{r},t)}{\partial t} =$$

$$\nabla\cdot\left(D_{\mathrm{p}}(\mathbf{r})\nabla C_{\mathrm{p}}(\mathbf{r},t)\right) - \lambda\left(1+\rho_{\mathrm{R}}\frac{(1-\varepsilon)}{\varepsilon}K_{\mathrm{d}}\right)C_{\mathrm{p}}(\mathbf{r},t). \qquad (53)$$

With the help of the definition (27) of the matrix retardation coefficient, (53) becomes

$$\frac{\partial C_{\mathrm{p}}(\mathbf{r},t)}{\partial t} = \nabla\cdot\left(\frac{D_{\mathrm{p}}(\mathbf{r})}{R_{\mathrm{p}}}\nabla C_{\mathrm{p}}(\mathbf{r},t)\right) - \lambda C_{\mathrm{p}}(\mathbf{r},t), \qquad (54)$$

which is the governing equation in the rock matrix.

## 4.6 Boundary and initial conditions

With the continuity and initial conditions

$$\begin{aligned} &C_{\mathrm{f}}(x,t) = C_{\mathrm{p}}(\mathbf{r},t); \quad |z| = b,\\ &C_{\mathrm{f}}(x=0,t) = C_0,\\ &C_{\mathrm{p}}(\mathbf{r},t=0) = 0, \end{aligned} \qquad (55)$$

the transport problem (41,54,55) is completely defined.

## 4.7 The transport model for a decay chain

When a decay chain is taken into account (see Chapter 4.3), the model in (41,54,55) for nuclide $C_{\mathrm{j}}$ takes the form

$$\begin{aligned} &R_{\mathrm{f,j}}\frac{\partial C_{\mathrm{f,j}}(x,t)}{\partial t} =\\ &\frac{\partial}{\partial x}\left(D_{\mathrm{f}}(x)\frac{\partial C_{\mathrm{f,j}}(x,t)}{\partial x}\right) - \frac{\partial}{\partial x}\left(v(x)C_{\mathrm{f,j}}(x,t)\right)\\ &+\frac{2}{2b}\left(\varepsilon D_{\mathrm{p}}(\mathbf{r})\frac{\partial C_{\mathrm{p,j}}(\mathbf{r},t)}{\partial z}\right)\Bigg|_{|z|=b} -\\ &-\lambda_{\mathrm{j}}R_{\mathrm{f,j}}C_{\mathrm{f,j}}(x,t) + \lambda_{\mathrm{j-1}}R_{\mathrm{f,j-1}}C_{\mathrm{f,j-1}}(x,t); \quad |z| = b, \end{aligned} \qquad (56)$$

$$\begin{aligned} &R_{\mathrm{p,j}}\frac{\partial C_{\mathrm{p,j}}(\mathbf{r},t)}{\partial t} = \nabla\cdot\left(D_{\mathrm{p}}(\mathbf{r})\nabla C_{\mathrm{p,j}}(\mathbf{r},t)\right)\\ &-\lambda_{\mathrm{j}}R_{\mathrm{p,j}}C_{\mathrm{p,j}}(\mathbf{r},t) + \lambda_{\mathrm{j-1}}R_{\mathrm{p,j-1}}C_{\mathrm{p,j-1}}(\mathbf{r},t), \end{aligned} \qquad (57)$$

with the continuity and initial conditions

$$\begin{aligned} &C_{\mathrm{f,j}}(x,t) = C_{\mathrm{p,j}}(\mathbf{r},t); \quad |z| = b,\\ &C_{\mathrm{f,j}}(x=0,t) = C_{0,\mathrm{j}},\\ &C_{\mathrm{p,j}}(\mathbf{r},t=0) = 0, \end{aligned} \qquad (58)$$

which is the most general transport model presented in this study. This model (56,57) has also been derived by K. Rasilainen in [9].

Analytical solutions can be found for problems for a single nuclide [5] and for a two-member decay chain [10]. This, however, calls for some additional simplifications to the model (56–58), which for a single nuclide will be presented in the following Chapter 4.8.

## 4.8 1D transport model for a single nuclide

**General assumptions**

General simplifying assumptions used in [5, p. 555–556] are the following.

- The fracture is thin and rigid with stationary characteristics.
- The fracture and the porous rock are saturated.
- The groundwater velocity in the fracture is constant and directed along the fracture ($x$-axis).
- At the origin of the fracture there exists a contaminant source of constant strength.
- Decay chains are not taken into account; the model is for a single nuclide.
- Water and rock characteristics, namely diffusion and coefficients $D_f$, $R_f$, $D_p$, $R_p$ and porosity $\varepsilon$ do not depend on position.

**Geometry and hydraulic properties**

Assumptions on the geometry and hydraulic properties used in [5, p. 556] are the following.

1. The width of the fracture is much smaller than its length.
2. Transverse diffusion and dispersion within the fracture assure complete mixing across the fracture width at all times.
3. The permeability of the porous matrix is very low and transport in the matrix occurs mainly by molecular diffusion.
4. Transport along the fracture is much faster than transport within the matrix.

Assumptions 1 and 2 provide the basis for a 1D representation of mass transport along the fracture itself. Assumption 3 and 4 furthermore provide the basis for taking the direction of mass flux density in the porous matrix to be perpendicular to the fracture axis. This results in the simplification of the basically 2D system to two orthogonal, coupled 1D systems.

**General 1D model for a single nuclide**

With the simplifications above, the model (56–58) becomes

$$\frac{\partial C_f(x,t)}{\partial t} = \frac{D_f}{R_f}\frac{\partial^2 C_f(x,t)}{\partial x^2} - \frac{v}{R_f}\frac{\partial C_f(x,t)}{\partial x} - \lambda C_f(x,t) + \frac{2}{2b}\frac{\varepsilon D_p}{R_f}\left.\frac{\partial C_p(x,z,t)}{\partial z}\right|_{|z|=b}; |z| = b, \tag{59}$$

$$\frac{\partial C_p(x,z,t)}{\partial t} = \frac{D_p}{R_p}\frac{\partial^2 C_p(x,z,t)}{\partial z^2} - \lambda C_p(x,z,t), |z| \geq b, \tag{60}$$

$$C_f(x,t) = C_p(x,z,t); \quad |z| = b, \tag{61}$$

$$C_f(x=0,t) = C_0, \tag{62}$$

$$C_p(x,z,t=0) = 0. \tag{63}$$

Conditions in infinity are

$$\lim_{x\to\infty} C_f(x,t) = 0, \tag{64}$$

$$\lim_{z\to\pm\infty} C_p(x,z,t) = 0. \tag{65}$$

The model (59–65) is the same as presented in [5, p. 557], except the inclusion of the absolute value of the $z$-co-ordinate, which takes into account the fact that diffusive loss occurs to both the fracture walls.

# 5 SOLUTIONS OF TRANSPORT MODELS

## 5.1 General 1D model for a single nuclide

The solution of the general 1D model (59–65) for a single nuclide is derived in [5, p. 557–559] to be

$$\frac{C_{\mathrm{f}}(x,t)}{C_0} = \frac{e^{\gamma x}}{\sqrt{\pi}} \int_l^{\infty} \left\{ e^{-\xi^2 - \frac{\gamma^2 x^2}{\xi^2}} e^{-\eta x^2} \left[ e^{-\sqrt{\lambda} Y} \operatorname{erfc}\left( \frac{Y}{2T} - \sqrt{\lambda} T \right) + e^{\sqrt{\lambda} Y} \operatorname{erfc}\left( \frac{Y}{2T} + \sqrt{\lambda} T \right) \right] \right\} d\xi, \tag{66}$$

$$\frac{C_{\mathrm{p}}(x,z,t)}{C_0} = \frac{e^{\gamma x}}{\sqrt{\pi}} \int_l^{\infty} \left\{ e^{-\xi^2 - \frac{\gamma^2 x^2}{\xi^2}} e^{-\eta x^2} \left[ e^{-\sqrt{\lambda} Y'} \operatorname{erfc}\left( \frac{Y'}{2T} - \sqrt{\lambda} T \right) + e^{\sqrt{\lambda} Y'} \operatorname{erfc}\left( \frac{Y'}{2T} + \sqrt{\lambda} T \right) \right] \right\} d\xi, \tag{67}$$

where
$\xi$ is a dummy integration variable and

$$l = \frac{x}{2} \sqrt{\frac{R_f}{D_f t}} \tag{68}$$

is the lower limit of integration. A sequence of other abbreviations used in (66,67) is

$$\gamma = v/(2D_{\mathrm{f}}), \tag{69}$$

$$\eta = \frac{\lambda R_{\mathrm{f}}}{4 D_{\mathrm{f}} \xi^2}, \tag{70}$$

$$Y = \frac{v^2 \beta^2}{4 A \xi^2} x^2, \tag{71}$$

$$Y' = \frac{v^2 \beta^2}{4 A \xi^2} x^2 + B(|z| - b), \tag{72}$$

$$T = \sqrt{t - \frac{v^2 \beta^2 x^2}{4\xi^2}} = \sqrt{t - \frac{R_{\mathrm{f}} x^2}{4 D_{\mathrm{f}} \xi^2}}, \tag{73}$$

in which

$$\beta^2 = 4 R_{\mathrm{f}} D_{\mathrm{f}} / v^2, \tag{74}$$

$$A = \frac{2b}{2} \frac{R_{\mathrm{f}}}{\varepsilon \sqrt{R_{\mathrm{p}} D_{\mathrm{p}}}}, \tag{75}$$

$$B = \sqrt{R_{\mathrm{p}} / D_{\mathrm{p}}}\,. \tag{76}$$

The use of the solution (66,67) involves numerical methods, namely, a search of the significant portion of the integration variable $\xi$ and a numerical integration at each calculation point ($x$,$z$).

## 5.2 1D model for a single nuclide with $D_f = 0$

Analytical solutions of partial differential equation systems can be derived with the help of *Laplace transformation*, some elementary rules of which are presented in Appendix 1. The solution of the 1D problem (59–65) for a single nuclide with $D_f = 0$ is derived in detail in Appendix 2. The result is

$$\frac{C_f(x,t)}{C_0} = 0, \quad t < t_0,$$

$$\frac{C_f(x,t)}{C_0} = \frac{1}{2} e^{-\lambda t_0} \left[ e^{-\frac{\sqrt{\lambda} t_o}{A}} \operatorname{erfc}\left( \frac{t_0}{2A\sqrt{t-t_0}} - \sqrt{\lambda(t-t_0)} \right) + e^{\frac{\sqrt{\lambda} t_o}{A}} \operatorname{erfc}\left( \frac{t_0}{2A\sqrt{t-t_0}} + \sqrt{\lambda(t-t_0)} \right) \right], \quad t > t_0, \tag{77}$$

$$\frac{C_p(x,z,t)}{C_0} = 0, \quad t < t_0,$$

$$\frac{C_p(x,z,t)}{C_0} = \frac{1}{2} e^{-\lambda t_0} \left[ e^{-\sqrt{\lambda} Z} \operatorname{erfc}\left( \frac{Z}{2\sqrt{t-t_0}} - \sqrt{\lambda(t-t_0)} \right) + e^{\sqrt{\lambda} Z} \operatorname{erfc}\left( \frac{Z}{2\sqrt{t-t_0}} + \sqrt{\lambda(t-t_0)} \right) \right], \quad t > t_0, \tag{78}$$

where

$$t_0 = \frac{R_f}{v} x, \tag{79}$$

$$Z = \frac{R_f}{vA} x + B(|z| - b) = \frac{t_0}{A} + B(|z| - b). \tag{80}$$

Equation (77) is used in the calculations of the present study in Chapters 7 and 8.

## 5.3 1D model for a single nuclide with $D_f = 0$, $\lambda = 0$

When the single nuclide is stable ($\lambda = 0$), (77,78) can be reduced to the form

$$\frac{C_f(x,t)}{C_0} = \operatorname{erfc}\left( \frac{t_0}{2A\sqrt{t-t_0}} \right), \quad t > t_0, \tag{81}$$

$$\frac{C_p(x,z,t)}{C_0} = \operatorname{erfc}\left( \frac{Z}{2\sqrt{t-t_0}} \right), \quad t > t_0. \tag{82}$$

When substituting (75,76,79,80), (81,82) become

$$\frac{C_f(x,t)}{C_0} = \operatorname{erfc}\left( \frac{\frac{R_f}{v} x}{2\frac{2b}{2}\frac{R_f}{\varepsilon\sqrt{R_p D_p}}\sqrt{t - \frac{R_f}{v} x}} \right) = \operatorname{erfc}\left( \frac{\varepsilon D_p x}{v 2b \sqrt{\frac{\varepsilon D_p}{\varepsilon R_p}\left( t - \frac{R_f}{v} x \right)}} \right), \quad t > \frac{R_f}{v} x, \tag{83}$$

$$\frac{C_p(x,z,t)}{C_0} = \mathrm{erfc}\left( \frac{\dfrac{R_f}{v\dfrac{2b}{2}\dfrac{R_f}{\varepsilon\sqrt{R_p D_p}}}x + \sqrt{R_p\ D_p}\left(|z|-b\right)}{2\sqrt{t-\dfrac{R_f}{v}x}} \right)$$

$$= \mathrm{erfc}\left( \frac{\varepsilon D_p x + \frac{1}{2}\left(|z|-b\right)v2b}{v2b\sqrt{\dfrac{\varepsilon D_p}{\varepsilon R_p}\left(t-\dfrac{R_f}{v}x\right)}} \right), \quad t > \frac{R_f}{v}x. \tag{84}$$

In VTT studies [2, p. 145], an effective diffusion coefficient has been defined to be

$$D_e = \varepsilon D_p, \tag{85}$$

where

$D_e$ is the effective diffusion coefficient from fracture to the matrix (m²/s).

With (85) and the definition of the groundwater transit time at $x$

$$t_w(x) = x/v, \tag{86}$$

where

$t_w$ is the groundwater transit time at $x$ (s),

the model (83,84) can be stated in the form

$$C_f(x,t) = C_p(x,z,t) = 0, \quad t \le t_w R_f, \tag{87}$$

$$\frac{C_f(x,t)}{C_0} = \mathrm{erfc}\left( \frac{D_e x}{v2b\sqrt{\dfrac{D_e}{\varepsilon R_p}\left(t-t_w(x)R_f\right)}} \right), \quad t > t_w(x)R_f, \tag{88}$$

$$\frac{C_p(x,z,t)}{C_0} = \mathrm{erfc}\left( \frac{D_e x + \frac{1}{2}\left(|z|-b\right)v2b}{v2b\sqrt{\dfrac{D_e}{\varepsilon R_p}\left(t-t_w(x)R_f\right)}} \right), \tag{89}$$

$t > t_w(x)R_f$,

which is equivalent to the illustrative model used in the VTT studies [2, p. 146]. The only difference is that the co-ordinate $z$ in [2] is replaced by $|z|-b$ in (89), which describes the effect of both the fracture surfaces and the aperture $2b$ (> 0) of the fracture.

## 5.4 The illustrative VTT model ($D_f = 0$, $\lambda = 0$)

In the VTT studies [2, p. 146; 1, p. 114] the illustrative model (87–89) is further manipulated and the calculations are done only for the fracture (88). The aim has been to study releases at a certain distance, say, $x = L$ (m), from the source of the contaminant. By applying (86) again, (88) can be stated in the form

$$\frac{C_f(L,t)}{C_0} = \mathrm{erfc}\left( \frac{D_e t_w(L)}{2b\sqrt{\dfrac{D_e}{\varepsilon R_p}\left(t-t_w(L)R_f\right)}} \right)$$

$$= \mathrm{erfc}\left( \frac{t_w(L)}{2b}\cdot\sqrt{\frac{\varepsilon D_e R_p}{\left(t-t_w(L)R_f\right)}} \right), \quad t > R_f t_w(L), \tag{90}$$

where

$L$ is a specific distance (m).

A further assumption is, that surface retardation and transit time can be neglected in the denominator of (90):

$$t - t_w(L)R_f \approx t. \tag{91}$$

This approximation also removes the fracture surface distribution coefficient $K_a$ from the model. According to VTT researchers [12], the distribution coefficients $K_d$ and $K_a$ can not be involved in the same model, because in the measurements they can not be distinguished.

With (91), (90) becomes

$$\frac{C_f(L,t)}{C_0} = \mathrm{erfc}\left( \frac{t_w(L)}{2b}\sqrt{\varepsilon D_e R_p}\cdot\sqrt{1\ t} \right)$$

$$= \mathrm{erfc}\left(u(L)\cdot t^{-1/2}\right), \quad t > R_f t_w(L), \tag{92}$$

where

$u$ is a parameter describing the properties of a transport route for a given species (s$^{1/2}$).

The $u$-parameter

$$u(L) = \sqrt{\varepsilon D_e R_p}\cdot\frac{t_w(L)}{2b}, \tag{93}$$

is a product of two terms. The first one is nuclide specific and takes into account the effects of matrix diffusion on the transport. The second factor is called the transport resistance. It does not depend on the nuclide, but it describes the groundwater flow distribution in the route. The transport resistance is usually presented in two alternative forms

$$R_T = \frac{t_w(L)}{2b} = \frac{W}{W}\frac{L}{v2b} = \frac{WL}{Q}, \quad (94)$$

where
$R_T$ is the transport resistance (s/m),
$W$ is the width of the flow channel (m),
$Q$ is the flow rate in the channel ($m^3/s$).

The first term of (93) is presented in [1, p. 115] differently for sorbing and non-sorbing species. For non-sorbing species $K_d$ is small and from (27) $R_p \approx 1$. For sorbing species $K_d$ is large and, consequently, $R_p \approx K_d\rho_R/\varepsilon$. The $u$-parameter is thus reduced to

$$u_{\text{non-sorbing}} = \sqrt{\varepsilon D_e} \cdot \frac{WL}{Q},$$
$$u_{\text{sorbing}} = \sqrt{D_e K_d \rho_R} \cdot \frac{WL}{Q}. \quad (95)$$

The parameters used in [1] and which need to be given values for modelling purposes are presented in (95) in their entirety: the matrix related $D_e$, $K_d$, $\rho_R$, $\varepsilon$, and flow channel related $WL/Q$.

# 6 VTT APPROACH

## 6.1 General

In TILA-99 [1], the whole research covers all the areas of release of nuclides including, e.g., activity content of a canister of spent fuel, modelling of the release of nuclides from the canister, transport in the near-field consisting of backfill of the deposition holes and tunnels and the excavation disturbed zone around the repository, modelling of the interface between the near-field and the geosphere, modelling of the geosphere transport, release from the geosphere according to various scenarios including dose-conversion, etc.

## 6.2 Model and data

The following is a summary of the approach to model geosphere transport and of the origin of the data used in TILA-99 [1, p. 114–120, 131–132].

**Illustrative model**

The conceptual model presented in TILA-99 gives the water phase concentration at a certain distance in a fracture for a case where a constant water phase concentration of a stable species is prevailing at the inlet of the fracture. The result is the equation (92). The characteristics of a transport route can thus be described by means of a single parameter ($u$) taking into account the effects of groundwater flow in the fracture system and the matrix diffusion, which is the only phenomenon considered to cause retardation and dispersion. The transport of the dissolved species is retarded when $u$ is increased.

In the transport resistance parameter (94), $WL$ represents the flow wetted surface. In TILA-99, a key phenomenon is the flow rate distribution in the fracture network, i.e., $W/Q$ and its integral along the transport path. In an advection–matrix diffusion model, the groundwater transit time is a meaningful parameter only when it is associated to a specific volume aperture.

Some phenomena which may increase retardation and dispersion and which are omitted in the analysis are the following: surface diffusion, sorption on fracture fillings, and diffusion from the flow channel into stagnant pools in the fracture in channelled flow. Route dispersion is not taken into account in the reference scenarios, either, because the emphasis is on the fastest possible flow channels from a repository to the biosphere.

**Sorption and matrix diffusion data**

Distribution coefficients in the rock matrix are defined for five sets of conditions in TILA-99:

1. **conservative values in reducing conditions in non-saline waters**,
2. **conservative values in reducing conditions in saline waters**,
3. realistic values in reducing conditions in non-saline waters,
4. realistic values in reducing conditions in saline waters,
5. conservative values in oxidising conditions in non-saline waters.

Only the cases 1–2 are used in the reference scenarios of TILA-99 and the $K_d$ values used for those cases for the nuclides involved in the calculations of the present study are presented in Table I. The $K_d$ value sets are based on the rock and groundwater types encountered at five investigation sites. For most elements the water composition is of much greater importance for sorption than the rock composition.

Natural analogues and laboratory experiments have shown pore connectivity over several tens of centimetres in the rock matrix. The penetration

***Table I.*** *Distribution coefficients ($K_d$) in the rock matrix ($m^3/kg$) [1, Table 11-9, p. 118] for the nuclides involved in the calculations of the present study.*

| Element | conservative non-saline reducing | conservative saline reducing |
|---|---|---|
| C | 0.0001 | 0.0001 |
| Cl | 0 | 0 |
| Ni | 0.1 | 0.005 |
| Se | 0.0005 | 0.0001 |
| Sr | 0.005 | 0.0001 |
| Zr | 0.2 | 0.2 |
| Nb | 0.02 | 0.02 |
| Tc | 0.05 | 0.05 |
| Pd | 0.001 | 0.0001 |
| Sn | 0.001 | 0.0001 |
| I | 0 | 0 |
| Cs | 0.05 | 0.01 |

may, however, be limited by sorption (which is incorporated in the model) and by the lower diffusivity in the unaltered rock matrix further away from the water-conducting fracture, which is taken into account by reducing the diffusivities by a factor of ten beyond one centimetre from the fracture. In the numerical model, the maximum penetration depth of matrix diffusion is limited to 10 cm due to computational reasons. The porosity and effective diffusion coefficient values used are presented in Table II. The density of the rock is taken to be 2700 $kg/m^3$.

**Transport resistance**

Transport resistance ($WL/Q$) values in TILA-99 have been calculated for several representative transport paths at each site that have been selected based on the flowpaths obtained in the regional-to-site scale groundwater flow analyses. The paths consist of excavation damaged zone, intact rock, fracture zones and combination of them. The results show no clear, systematic differences between the sites. The differences in the obtained $WL/Q$ values are related more to the details of the analysed preliminary repository layouts than to the site properties of the bedrock.

The lower range of the estimated $WL/Q$ values are close to those used in studies prior to TILA-99, whereas the maximum values are significantly higher than those used in the previous safety assessments on crystalline rock. $WL/Q$ values of the order of $10^6$ yr/m would result in negligible releases into the biosphere.

There are significant conceptual and parameter uncertainties related to the modelling of flow and transport especially in the excavation damaged zone and fracture zones. Taking these uncertainties into consideration, the following $WL/Q$ values have been selected for use in TILA-99:

- "median" $WL/Q$ for all sites: $5\times10^4$ a/m. Considering that $WL/Q = t_w/2b$, the value can be illustrated as follows: With a volume aperture of $2b = 5\times10^{-4}$ m, it corresponds to a groundwater transit time $t_w = 25$ a. Secondly, assuming a flow channel with a width of $W = 0.1$ m and a length of $L = 600$ m, the flow rate is $Q = 1.2$ l/a,
- "95$^{th}$ percentile" for all sites: $2\times10^4$ a/m (with the above assumptions, this corresponds to $t_w$ = 10 a and $Q = 3$ l/a),
- very high flow in saline conditions: $1\times10^4$ a/m ($t_w = 5$ a, $Q = 6$ l/a),
- very high flow in non-saline conditions: $5\times10^3$ a/m ($t_w = 2.5$ a, Q = 12 l/a).

**FTRANS code**

The transport analyses in TILA-99 are performed with the FTRANS code [13], which can take into account decay chains and the heterogeneity of the

***Table II.*** *Porosity ε (-) and effective diffusion coefficient $D_e$ ($m^2/s$) in the rock. C, Cl, Se, Pd, Sn, and I are assumed to appear as anions in all cases; Tc (U, Pu, Np) in oxidising conditions [1, Table 11-10, p. 120].*

| | Distance from the fracture 0–1 cm | | Distance from the fracture 1–10 cm | |
|---|---|---|---|---|
| | ε (–) | $D_e$ ($m^2/s$) | ε (–) | $D_e$ ($m^2/s$) |
| **Non-anions** | | | | |
| **non-saline and saline groundwater** | 0.005 | $1 \cdot 10^{-13}$ | 0.001 | $1 \cdot 10^{-14}$ |
| **Anions** | | | | |
| **non-saline groundwater** | 0.001 | $1 \cdot 10^{-14}$ | 0.0002 | $1 \cdot 10^{-15}$ |
| **Anions** | | | | |
| **saline groundwater** | 0.002 | $5 \cdot 10^{-14}$ | 0.0004 | $5 \cdot 10^{-15}$ |

rock matrix adjacent to the water-conducting fracture. FTRANS is a dual-porosity model, which employs the conventional parameters for advection along the fracture:

- length of the transport path,
- velocity of the water flowing in the fracture and
- aperture of the fracture.

These input parameters are fixed in TILA-99 in such a way that the chosen value for the primary input parameter transport resistance $R_T$ (94) is obtained.

***Table III.*** *Half lives of the nuclides involved in the calculations of the present study [1, p. 21]*

| Nuclide | $T_{½}$ (a) |
|---|---|
| C-14 | $5.7 \cdot 10^3$ |
| Cl-36 | $3.0 \cdot 10^5$ |
| Ni-59 | $8.0 \cdot 10^4$ |
| Ni-63 | $9.6 \cdot 10^1$ |
| Se-79 | $6.4 \cdot 10^4$ |
| Sr-90 | $2.9 \cdot 10^1$ |
| Zr-93 | $1.5 \cdot 10^6$ |
| Nb-94 | $2.0 \cdot 10^4$ |
| Tc-99 | $2.1 \cdot 10^5$ |
| Pd-107 | $6.5 \cdot 10^6$ |
| Sn-126 | $1.0 \cdot 10^5$ |
| I-129 | $1.6 \cdot 10^7$ |
| Cs-135 | $2.3 \cdot 10^6$ |
| Cs-137 | $3.0 \cdot 10^1$ |

# 7 CALCULATIONS

## 7.1 Different approaches—implications to choice of parameter values

Both the approaches of TILA-99 and the present study employ a geosphere transport model in which the same phenomena are incorporated. Main differences between the calculation model used in this report (77) and the FTRANS code used in TILA-99 by VTT are collected in Table IV.

The most considerable difference between the approaches is the doubly finite domain used in TILA-99 and the infinite domain used in the present study. VTT has used different parameter values for each domain in TILA-99 (Table II) and only single values can be used in the approach of the present study.

According to a correspondence with T. Vieno and H. Nordman of VTT, the nuclides can be divided into two categories according to their values of distribution coefficient $K_d$. The parameter values for the 0–1 cm zone of the rock can be used for the retarding nuclides for which $K_d > 1 \cdot 10^{-4}$, because they are mainly retarded in this zone. On the other hand, for the weakly or non-retarding nuclides for which $K_d \leq 1 \cdot 10^{-4}$ the parameter values for the 1–10 cm zone of the rock can be used. This division is rough, of course, and the behaviour of an output does not depend solely on the $K_d$ value but also, e.g., on the shape of the input. [14]

The rock parameter values in this study are chosen to be the same as in TILA-99 as presented in Table II. $K_d$ is chosen nuclide specifically according to the groundwater chemistry (Table I). The values of rock parameters $D_e$ and $\varepsilon$ depend on the chemical nature of the nuclide, the groundwater salinity and the $K_d$ value. The density of rock is always $\rho_R = 2700$ kg/m$^3$.

The transport resistance gets the value $WL/Q = t_w/2b = 5 \cdot 10^4$ a/m in the base cases. With a volume aperture of $2b = 5 \cdot 10^{-4}$ m, it corresponds to a groundwater transit time $t_w = 25$ a.

## 7.2 Sensitivity analysis for transport resistance

To investigate the influence of the transport resistance on the result the value of it is varied for some nuclides in a particular case. In TILA-99 the transport resistance is given the values $WL/Q \in [5 \cdot 10^3, 5 \cdot 10^4]$ a/m, which according to VTT is a rather conservative range [1, p. 132]. When the aperture is kept constant ($2b = 5 \times 10^{-4}$ m), this corresponds to a transit time range $t_w \in [2.5 \cdot 10^0, 2.5 \cdot 10^1]$ a.

In TILA-99, this range of values is chosen according to data obtained by measurements and simulations [1, p. 131–132]. The extrema of these estimated values $WL/Q \in [2.2 \cdot 10^2, 1.1 \cdot 10^7]$ a/m are not realistic. In this study, we have chosen two values used in TILA-99 corresponding to the "median" $WL/Q = 5 \cdot 10^4$ a/m and the "very high flow in saline conditions" $WL/Q = 1 \cdot 10^4$ a/m cases. Additionally, two values are chosen beyond this range but within the range of the measurement and simulation estimates of TILA-99 to assess the effect of this parameter. In our analytical approach, the variation is done by keeping the aperture constant and varying the transit time. The transport resistance values and the corresponding transit time range used in the present study are presented in Table V.

***Table IV.*** *The main differences between the calculation model used in this report and the FTRANS code used in TILA-99 by VTT*

| This report; equation (77) | TILA-99; FTRANS |
|---|---|
| Analytical model | Numerical model — discretisations |
| Infinite domain with single rock parameter values | Two finite domains with differing rock parameter values |
| $R_T = WL/Q = t_w/2b$ is given by means of $t_w$ and $2b$ | $R_T = WL/Q = t_w/2b$ is given by means of L, Q (v) and $2b$ [1, p. 120] |
| Single nuclide | Decay chains |

## 7.3 Chosen cases

**SH-sal50 and DC-ns50 scenarios of TILA-99**

In TILA-99 [1, p. 135–147], a detailed analysis of two scenarios is presented:

1. SH-sal50, i.e., small initial hole in the canister, median flow and transport data, saline groundwater and
2. DC-ns50, i.e., canister disappearing at 10 000 years, median flow and transport data, non-saline groundwater.

The detailed presentation of the results in these two scenarios in TILA-99 is aimed to highlight the key features of the release and transport of radionuclides. The results are for a single canister containing 2.14 tU spent fuel from the Olkiluoto reactors.

The actual data of these cases presented in TILA-99 was received from VTT to be exploited in the present study [14]. Because our analytical model can not handle decay chains, we have chosen some single nuclides from among the nuclides involved in these cases of the TILA-99 analysis. These nuclides are

- C-14, Cl-36, Ni-59, Ni-63, Se-79, Sr-90, Nb-94, Tc-99, Sn-126, I-129, Cs-135 and Cs-137 in SH-sal50 scenario and
- C-14, Cl-36, Ni-59, Se-79, Zr-93, Zr-93f, Nb-94, Tc-99, Pd-107, Sn-126, I-129 and Cs-135 in DC-ns50 scenario.

***Table V.*** *The transport resistance values WL/Q (a/m) and the corresponding transit time range $t_w$ (a) used in the sensitivity analysis of the present study*

| *WL/Q* (a/m) | $t_w$ (a) |
|---|---|
| $1.0 \cdot 10^3$ | 0.50 |
| $1.0 \cdot 10^4$ | 5.0 |
| $5.0 \cdot 10^4$ | 25 |
| $5.0 \cdot 10^5$ | 50 |

The TILA-99 data for these cases are presented in Figure 4 and Table VI for SH-sal50 and in Figure 5 and Table VII for DC-ns50. In cases where the release pulse is solubility-limited or otherwise very flat, $t_{max}$ of the TILA-99 results presented in the tables is actually the time when the pulse reaches 90% of the maximum level.

The release rates from the near field to the geosphere is from now on referred to as the "input". The results, i.e., release rates from geosphere to biosphere are from now on referred to as the "output". The TILA-99 inputs are plotted by blue, TILA-99 outputs by red and the outputs of the present study by black.

The half lives of the nuclides involved in this study are presented in Table III.

**Sensitivity analysis**

For variation of $t_w$ the results are calculated for three nuclides of different type

- non-retarding Cl-36,
- retarding Ni-59,
- quickly decaying Sr-90.

The variant cases are based on the SH-sal50 scenario.

## 7.4 The calculation program

The solutions derived in the present study are for a constant infinite inlet condition i.e. for a step input. In computations, an output for a finite rectangular pulse with a duration DT(a) can be constructed by calculating the difference of outputs of two identical step inputs shifted DT from apart [3].

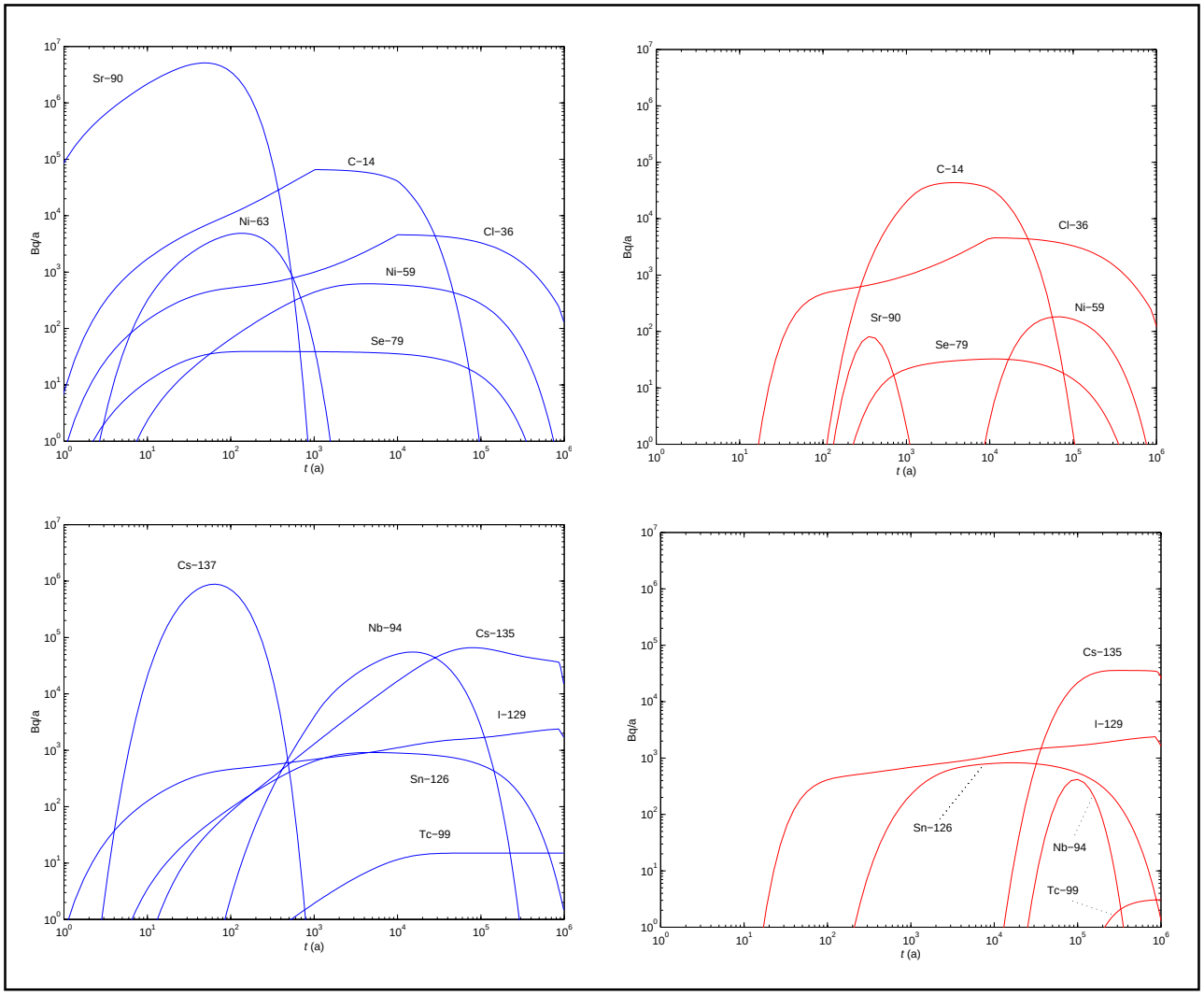


***Figure 4.*** *Release rates of activation and fission products from the near-field into the geosphere (left) and from the geosphere into the biosphere (right) in the SH-sal50 scenario [1, Figure 11-5, p. 137].*

An output for a more arbitrary input can be constructed by approximating the input by rectangular pulses of given height (release rate (Bq/a)) and width (duration (a)). In practice, this is natural, because this kind of an arbitrary input pulse is given in a vector form (not in a functional form), in which the widths and the heights are readily presented.

The program receives a release rate vector and the corresponding time vector as an input, treats this data as individual rectangular inputs, calculates the individual outputs of these inputs and gives the final result output as the sum of the individual outputs.

The program is presented in more detail in Appendices 8 and 9.

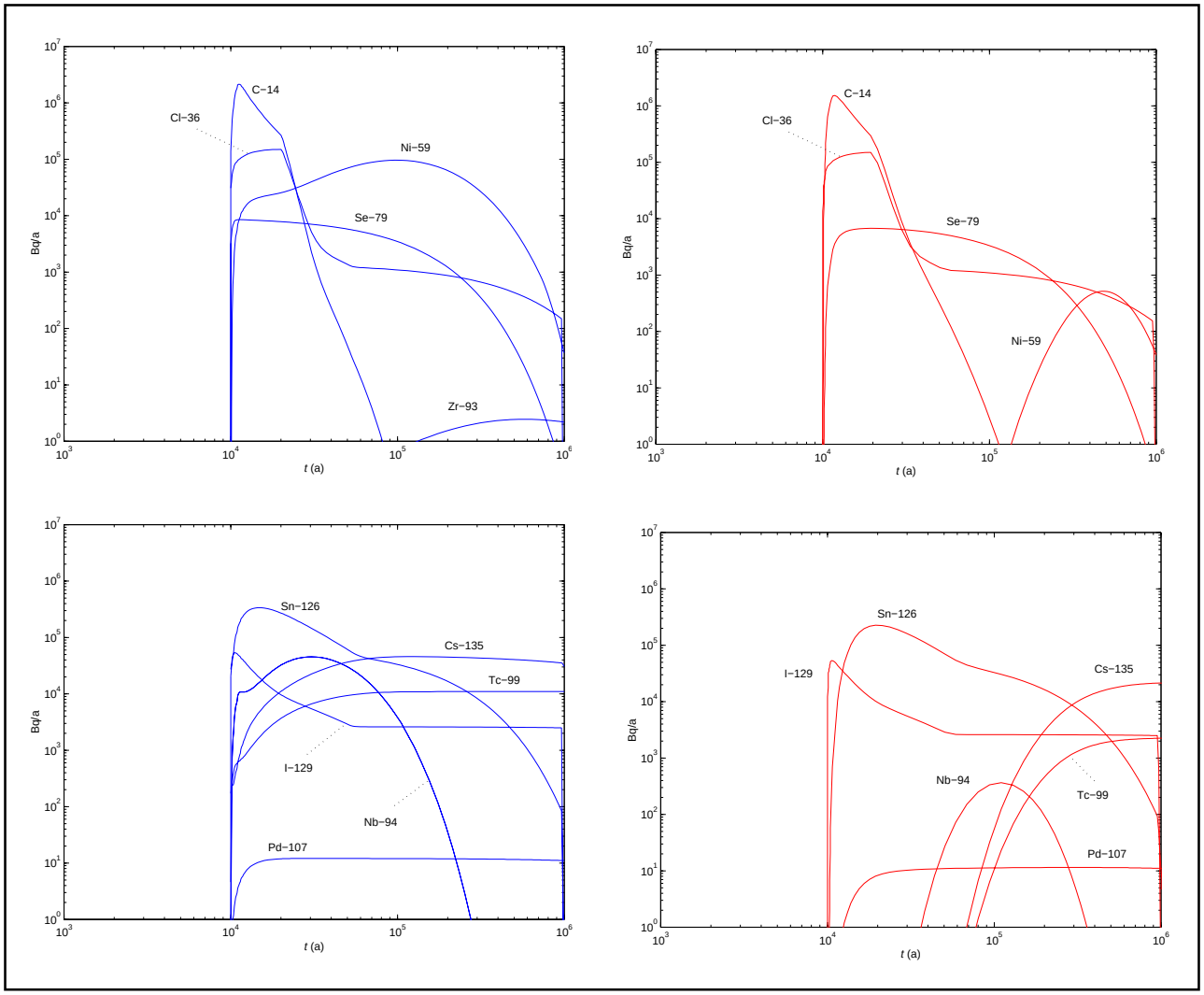


***Figure 5.*** *Release rates of activation and fission products from the near-field into the geosphere (left) and from the geosphere into the biosphere (right) in the DC-ns50 scenario [1, Figure 11-9, p. 141].*

# 8 RESULTS

## 8.1 SH-sal50 and DC-ns50 scenarios

The significant result outputs of the SH-sal50 scenario with the corresponding TILA-99 results are presented in Figure 6. Nuclide specific results with TILA-99 inputs and outputs are presented in Appendices 3 and 4. Maximum release rates with the TILA-99 results are presented in Table VI.

The significant result outputs of the DC-ns50 scenario with the corresponding TILA-99 results are presented in Figure 7. Nuclide specific results with TILA-99 inputs and outputs are presented in Appendices 5 and 6. Zr-93f is a separate case and not plotted together with the other cases in Figure 7. Maximum release rates with the TILA-99 results are presented in Table VII.

The cases for which the result of the present study was insignificant ($< 10^0$) are plotted in Appendix 7. In those figures, the whole input and output of the TILA-99 results and the shapes of the results of the present study are shown.

***Table VI.*** *Maximum release rates (Bq/a) from geosphere in SH-sal50 scenario – TILA-99 results [1, Table 11-20, p. 136] and the results of the present study.*

| | TILA-99 | | The present study | |
|---|---|---|---|---|
| Nuclide | $t_{max}$(a) | (Bq/a) | $t_{max}$(a) | (Bq/a) |
| C-14 | $3.8 \cdot 10^3$ | $4.4 \cdot 10^4$ | $4.0 \cdot 10^3$ | $4.5 \cdot 10^4$ |
| Cl-36 | $9.4 \cdot 10^3$ | $4.6 \cdot 10^3$ | $1.1 \cdot 10^4$ | $4.6 \cdot 10^3$ |
| Ni-59 | $7.0 \cdot 10^4$ | $1.8 \cdot 10^2$ | $1.4 \cdot 10^5$ | $4.3 \cdot 10^1$ |
| Ni-63 | — | — | — | — |
| Se-79 | $3.2 \cdot 10^3$ | $3.3 \cdot 10^1$ | $9.0 \cdot 10^3$ | $3.1 \cdot 10^1$ |
| Sr-90 | $3.5 \cdot 10^2$ | $8.1 \cdot 10^1$ | $1.9 \cdot 10^2$ | $2.3 \cdot 10^4$ |
| Nb-94 | $1.0 \cdot 10^5$ | $4.2 \cdot 10^2$ | $1.3 \cdot 10^5$ | $1.1 \cdot 10^1$ |
| Tc-99 | $5.2 \cdot 10^5$ | $3.1 \cdot 10^0$ | — | — |
| Sn-126 | $5.5 \cdot 10^3$ | $8.3 \cdot 10^2$ | $1.0 \cdot 10^4$ | $7.8 \cdot 10^2$ |
| I-129 | $4.2 \cdot 10^5$ | $2.4 \cdot 10^3$ | $8.5 \cdot 10^5$ | $2.4 \cdot 10^3$ |
| Cs-135 | $1.8 \cdot 10^5$ | $3.6 \cdot 10^4$ | $9.2 \cdot 10^5$ | $1.9 \cdot 10^4$ |
| Cs-137 | — | — | — | — |

***Table VII.*** *Maximum release rates (Bq/a) from geosphere in DC-ns50 scenario – TILA-99 results [1, Table 11-21, p. 140] and the results of the present study.*

| | TILA-99 | | The present study | |
|---|---|---|---|---|
| Nuclide | $t_{max}$(a) | (Bq/a) | $t_{max}$(a) | (Bq/a) |
| C-14 | $1.2 \cdot 10^4$ | $1.5 \cdot 10^6$ | $1.2 \cdot 10^4$ | $1.7 \cdot 10^6$ |
| Cl-36 | $1.5 \cdot 10^4$ | $1.5 \cdot 10^5$ | $2.0 \cdot 10^4$ | $1.5 \cdot 10^5$ |
| Ni-59 | $4.9 \cdot 10^5$ | $5.2 \cdot 10^2$ | $5.9 \cdot 10^5$ | $9.0 \cdot 10^1$ |
| Se-79 | $1.5 \cdot 10^4$ | $6.8 \cdot 10^3$ | $2.3 \cdot 10^4$ | $4.9 \cdot 10^3$ |
| Zr-93 | — | — | — | — |
| Zr-93f | $1.0 \cdot 10^6$ | $2.2 \cdot 10^2$ | — | — |
| Nb-94 | $1.1 \cdot 10^5$ | $3.7 \cdot 10^2$ | $1.4 \cdot 10^5$ | $9.5 \cdot 10^0$ |
| Tc-99 | $5.5 \cdot 10^5$ | $2.3 \cdot 10^3$ | $1.2 \cdot 10^6$ | $2.5 \cdot 10^2$ |
| Pd-107 | $3.4 \cdot 10^4$ | $1.2 \cdot 10^1$ | $4.5 \cdot 10^5$ | $1.1 \cdot 10^1$ |
| Sn-126 | $1.9 \cdot 10^4$ | $2.3 \cdot 10^5$ | $2.2 \cdot 10^4$ | $1.5 \cdot 10^5$ |
| I-129 | $1.1 \cdot 10^4$ | $5.3 \cdot 10^4$ | $1.1 \cdot 10^4$ | $5.3 \cdot 10^4$ |
| Cs-135 | $6.5 \cdot 10^5$ | $2.2 \cdot 10^4$ | $1.2 \cdot 10^6$ | $5.7 \cdot 10^3$ |

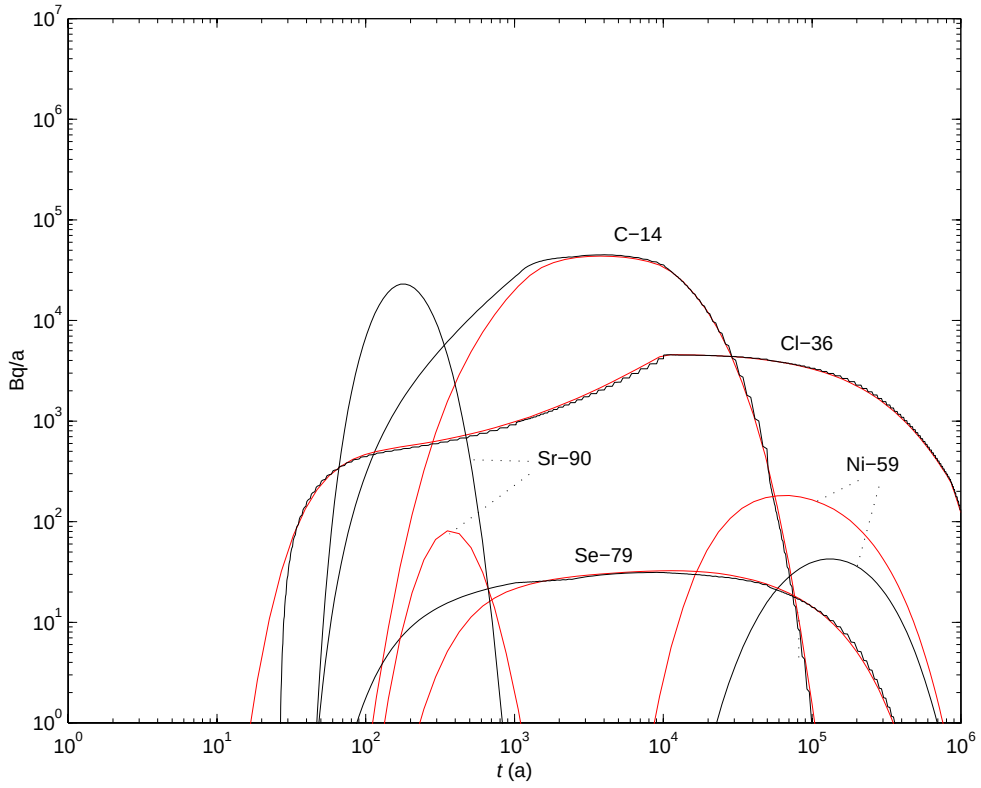


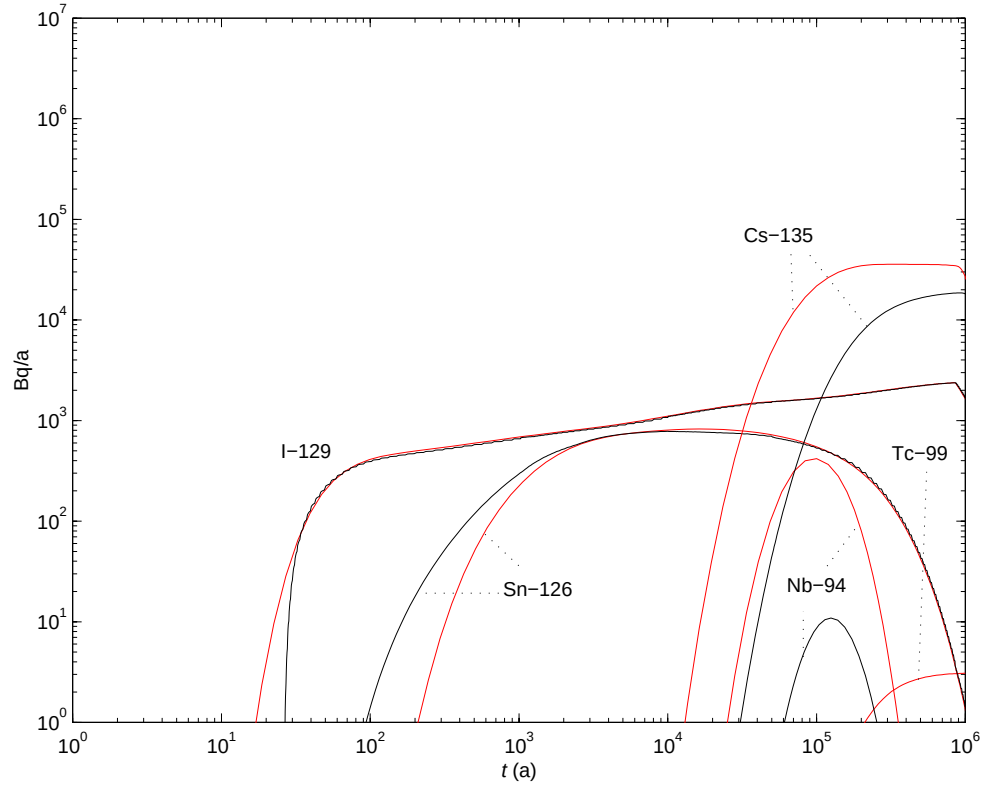


***Figure 6.*** *Release rates of fission and activation products in SH-sal50 scenario.*
***Red****: TILA-99 output;* ***Black****: Result output of the present study.*

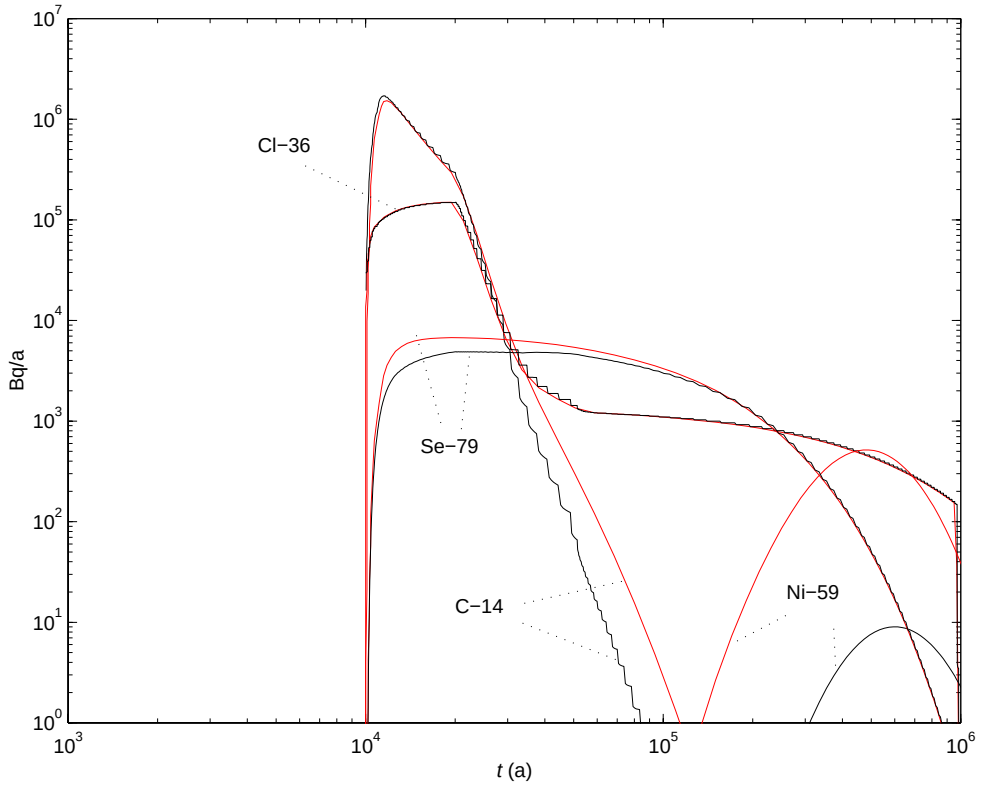


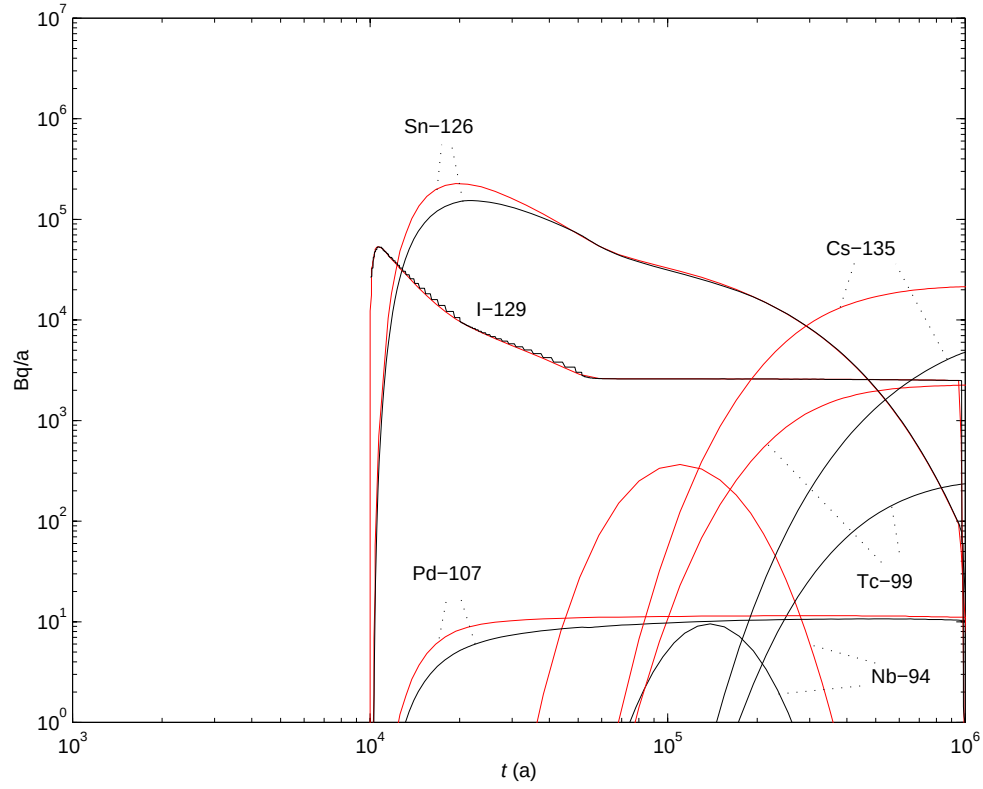


***Figure 7.*** *Release rates of fission and activation products in DC-ns50 scenario.*
***Red****: TILA-99 output;* ***Black****: Result output of the present study.*

***Table VIII.*** *Maximum release rates (Bq/a) for various values of $t_w$ (a) in cases based on the SH-sal50 scenario.*

| | Cl-36 | | Ni-59 | | Sr-90 | |
|---|---|---|---|---|---|---|
| $t_w$(a) | $t_{max}$(a) | (Bq/a) | $t_{max}$(a) | (Bq/a) | $t_{max}$(a) | (Bq/a) |
| 0.5 | $1.1 \cdot 10^4$ | $4.6 \cdot 10^3$ | $7.8 \cdot 10^3$ | $5.6 \cdot 10^2$ | $5.6 \cdot 10^1$ | $4.6 \cdot 10^6$ |
| 5 | $1.1 \cdot 10^4$ | $4.6 \cdot 10^3$ | $3.4 \cdot 10^4$ | $3.0 \cdot 10^2$ | $8.2 \cdot 10^1$ | $1.7 \cdot 10^6$ |
| [a] 25 | $1.1 \cdot 10^4$ | $4.6 \cdot 10^3$ | $1.4 \cdot 10^5$ | $4.3 \cdot 10^1$ | [b] $1.7 \cdot 10^2$ | $2.3 \cdot 10^4$ |
| 50 | $1.1 \cdot 10^4$ | $4.5 \cdot 10^3$ | $2.5 \cdot 10^5$ | $4.9 \cdot 10^0$ | $2.9 \cdot 10^2$ | $1.2 \cdot 10^2$ |

[a] equivalent to the SH-sal50 scenario

[b] the calculation lattice for Sr-90 with $t_w$ = 25 a is different from that in the SH-sal50 case in Table VI

## 8.2 Sensitivity analysis

The result outputs of Cl-36, Ni-59, and Sr-90, when $t_w$ is varied in cases based on the SH-sal50 scenario are presented in Figure 8. Maximum release rates for each value of $t_w$ are presented in Table VIII.

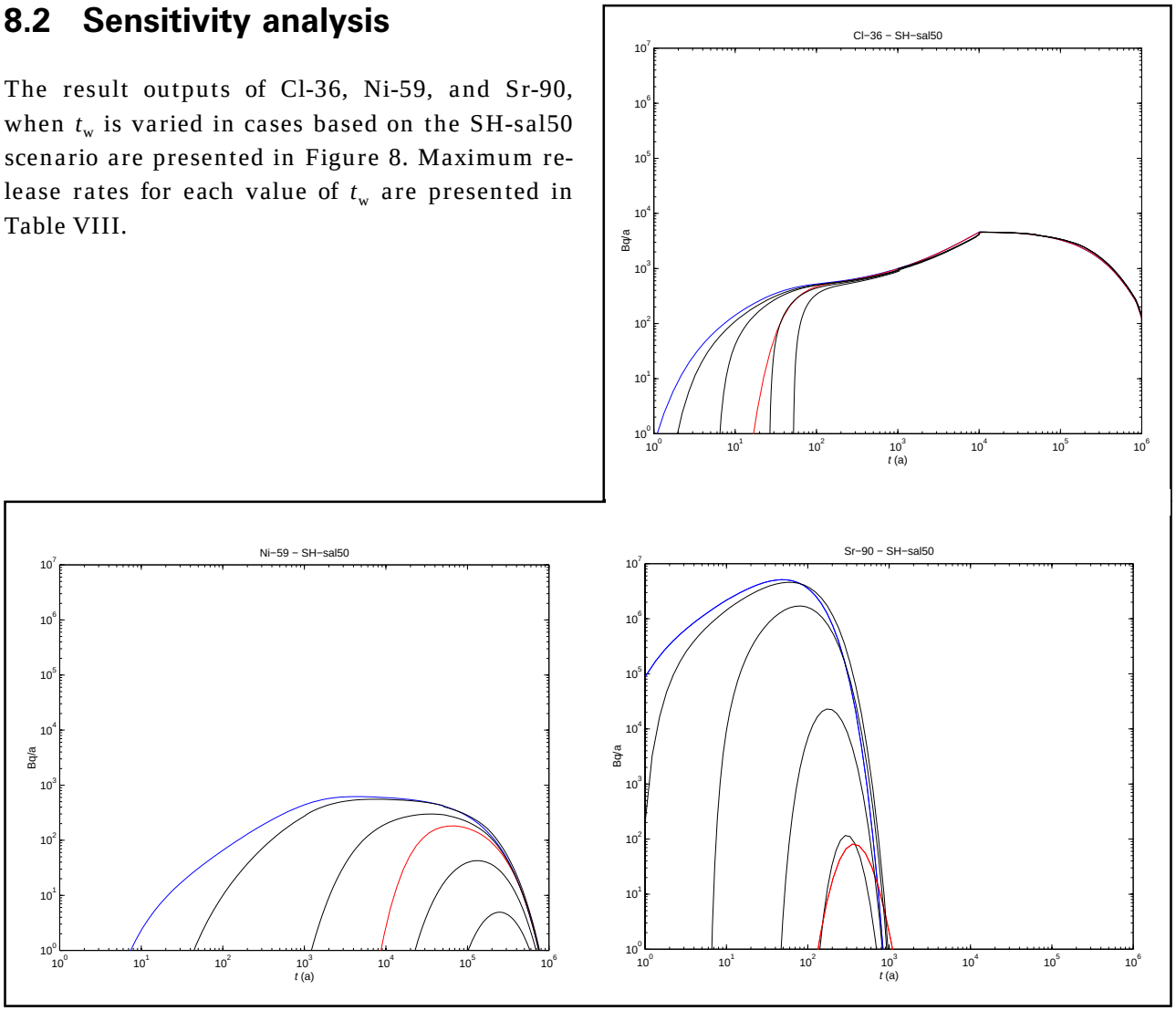


***Figure 8.*** *Variation of transit time in cases based on the SH-sal50 scenario.* ***Blue:*** *TILA-99-input;* ***Red:*** *TILA-99-output;* ***Black*** *(from left to right in each figure): $t_w$ = 0.5, 5, 25, 50 a.*

# 9 REVIEW OF THE RESULTS

## 9.1 General

The results for the SH-sal50 and DC-ns50 scenarios are quite similar to those in TILA-99. In this chapter, reasons for the deviations are discussed mainly on the basis of the differences in the calculation approaches.

## 9.2 Rock parameters

The parameter values of intact rock were used for weakly and non-retarding nuclides whereas the parameter values of more porous altered rock zone were used for more retarding nuclides. I.e., for weakly and non-retarding nuclides the rock was generally more solid and for retarding nuclides generally more porous when compared to the TILA-99 calculations. Consequently, the weakly and non-retarding nuclides should diffuse and be retarded less and the retarding nuclides should diffuse and be retarded more in the present approach compared to the TILA-99 calculations.

The expected result is, that the outputs of the weakly and non-retarding nuclides

- C-14, Cl-36, Se-79, Sr-90, Pd-107, Sn-126 and I-129 in SH-sal50 scenario and
- C-14, Cl-36 and I-129 in DC-ns50 scenario

should be larger and/or less retarded than the corresponding TILA-99 outputs and the outputs of the retarding nuclides

- Ni-59, Ni-63, Nb-94, Tc-99, Cs-135 and Cs-137 in SH-sal50 scenario and
- Ni-59, Se-79, Zr-93, Zr-93f, Nb-94, Tc-99, Pd-107, Sn-126, and Cs-135 in DC-ns50 scenario

are expected to be smaller and/or more retarded than the corresponding TILA-99 outputs.

This theoretical expectation is fulfilled by all the results in Figures 6 and 7, Appendices 3–7, and Tables VI and VII.

In this respect, the employment of the rock parameter values seems to be one clear cause of the distinction between the results of TILA-99 and the present study. This effect can be further assessed by interchanging the rock parameter values, i.e., by giving weakly retarding nuclides the values of altered rock and the retarding nuclides the values of intact rock. In Figure 9 this is done for some nuclides of various retardation type in both scenarios. It can be seen that the TILA-99 results occur in between the previous results and the results for interchanged rock parameter values, which was also expected. This strengthens the assumption that the differences between the results of the present study and TILA-99 can to a considerable extent be explained by means of the given rock parameter values.

A questionable case is the weakly sorbing C-14 in the DC-ns50 scenario in Figure 7 and Appendix 5, for which the TILA-99 output is mostly over the output of the present study. However, because of the larger maximum of the output of the present study (Table VII), the area under the release rate curve of the result of the present study is larger than under the TILA-99 curve, which means that the total release associated with the result of the present study is larger, as expected. This is not clearly seen because of the logarithmic scale used in the figures. In any case, the difference is small and can also be partly explained by the rectangular approximation of the input pulse used in the present study (Chapter 9.3) or by the shape of the input.

The results of TILA-99 for sorbing species, e.g., Ni-59 in Figure 9, differ approximately as much from the results of the base cases and the cases where the rock parameter values are interchanged between the rock zones. This implies, that the rough estimation that the nuclides for which $K_d$ >

$1 \cdot 10^{-4}$ see essentially only the altered rock zone is, indeed, too rough. The effective penetration depth for these sorbing nuclides seems to be beyond the altered rock zone of one centimetre.

However, according to T. Vieno of VTT, too far reaching nuclide specific conclusions must not be made, because the result can depend considerably on the shape of the input. There are cases in which the output is dominated by the source term, i.e., in which the output is almost identical with the input. These cases are long-lived, weakly retarding nuclides, whose input is flat. In such cases the result does not give any information of the details of the geosphere transport. In the case of non-retarding nuclides also the limit set to the penetration depth (10 cm) affects the solution, i.e., in the analytical approach of the present study, these nuclides penetrate even deeper.[15]

## 9.3 Rectangular approximation of the input

For weakly and non-sorbing nuclides the effect of the rectangular approximation of the input is the most noticeable. If the calculation lattice is dense (the lattice parameter N_DTi is large in the program (Appendix 9 (1/4))), the outputs of the individual rectangular input pulses are also quite edgy and do not overlap considerably. Consequently, the summed result outputs are also edgy, see, e.g., I-129, Cl-36, and C-14 in Figures 6 and 7.

On the contrary, for sorbing nuclides the outputs of the individual rectangular input pulses get significant values in most cases only after $t = t_w + DT$ years after the beginning of the respective individual input pulse. Consequently, the individual output pulses overlap, the summed result outputs are smooth and there is no need for a dense calculation lattice.

The calculation lattice parameter values have also a marginal effect on the result. E.g., $t_{max}$ for Sr-90 in Table VI and in Table VIII for the transit time $t_w = 25$ a deviates a little although the case is the same. This is due to a slight difference in the values of calculation lattice parameters used in those cases.

## 9.4 Analytical vs. numerical model—flow parameters

Strong conclusions on this kind of difference can not be stated in general. A numerical approach is often sensitive to discretisations, a situation of which is often assessed by comparing to analytical solutions. The behaviour of the result of an analytical model is more predictable without calculations. An analytical model can give well-behaving continuous results even for cases where the result is not numerically significant (see, e.g., Appendix 7). Of course, if the result for an analytical model is calculated by a computer, precision of the calculation can cause irregularities.

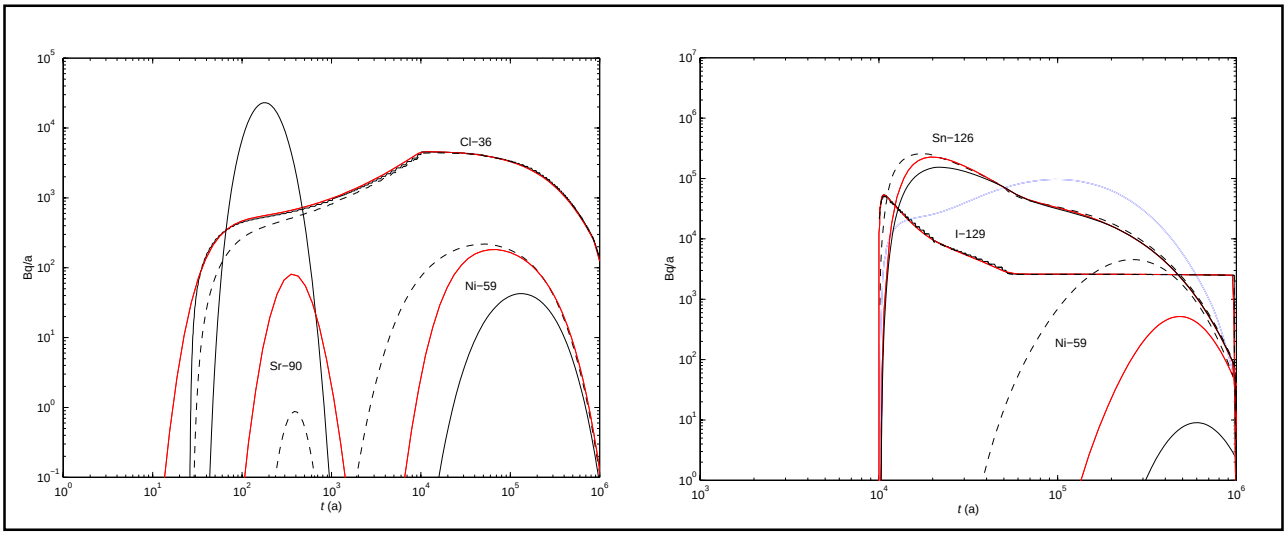


***Figure 9.*** *Release rates of Cl-36, Ni-59 and Sr-90 in the SH-sal50 scenario (left) and Ni-59, Sn-126 and I-129 in the DC-ns50 scenario (right).* ***Red****: TILA-99 output;* ***Black****: Present result; Dashed: Present result with the rock parameters interchanged between the rock zones.*

In Figure 10, early values of Cl-36 and Se-79 outputs in SH-sal50 scenario (compare to Figure 6 and Appendix 3) indicate the different approaches to employ the flow parameters within the transport resistance parameter. The analytical solutions begin always at $t = t_w$ (= 25 a in this situation) after the beginning of the input pulse, while in the TILA-99 results, a continuous well-behaving solution can be seen to start earlier in these cases. In an analytical model with $t_w$ as an individual input parameter, such a case is impossible if there is no longitudinal dispersion incorporated in the model.

## 9.5 Variation of the transport resistance

The value of $t_w$ has a considerable effect for some nuclides (Figure 8). The effect is the most significant in the case of quickly retarding Sr-90. The effect is the smallest for the non-retarding Cl-36, for which only the starting point of the output is shifted as $t_w$.

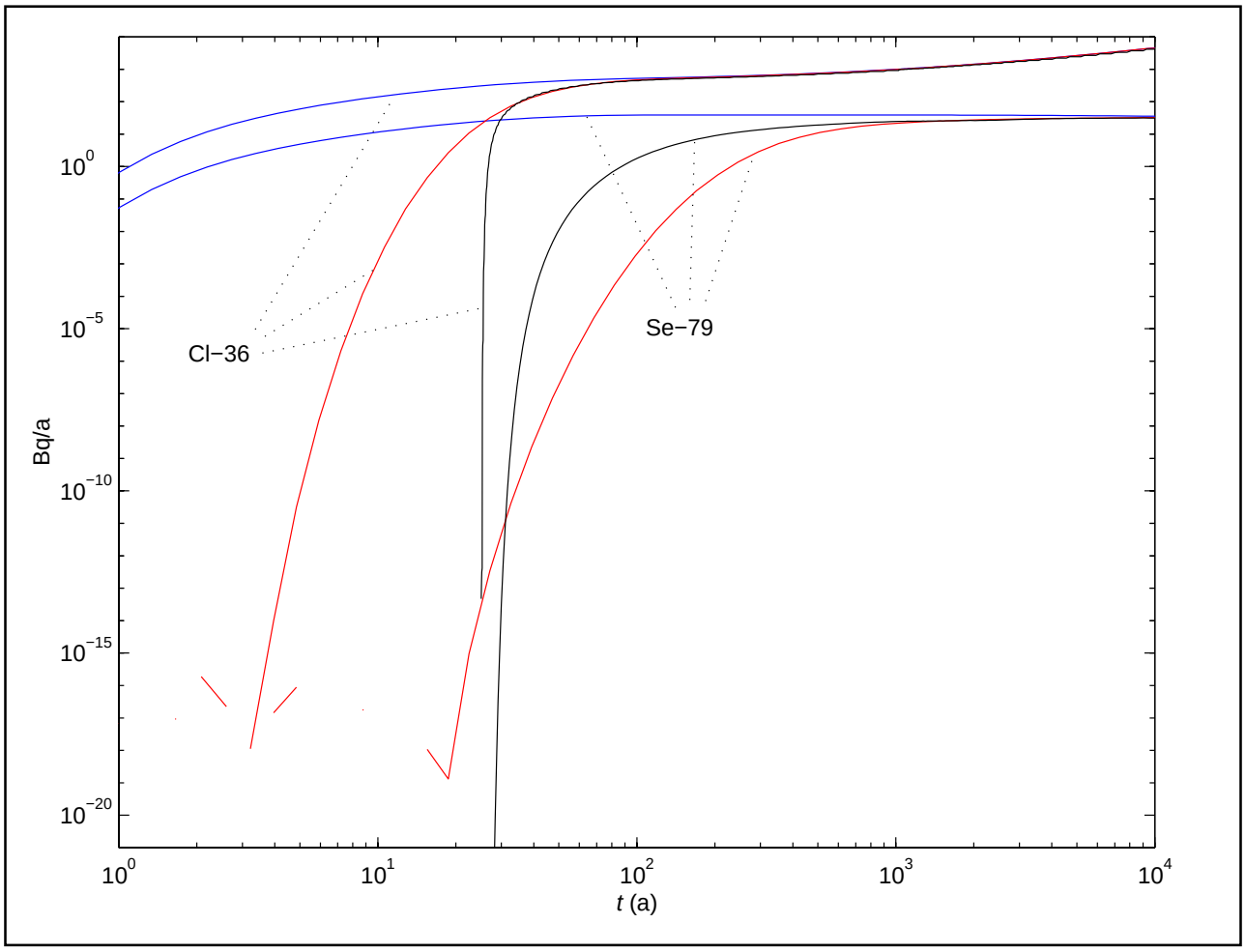


***Figure 10.*** *Release rates of Cl-36 and Se-79 in the SH-sal50 scenario—early values of the results.* ***Blue****: TILA-99 input;* ***Red****: TILA-99 output;* ***Black****: Present result.*

# 10 DISCUSSION

Radionuclide transport models via a heat transfer analogy and solutions of them were derived. The calculations were done for a single nuclide model for which the following processes were taken into account:

- advective transport along the fracture,
- diffusion from the fracture into and within the rock matrix,
- retardation within the matrix and
- radioactive decay.

The results were compared to the results of the same calculation cases obtained by VTT and presented in TILA-99 safety assessment report. In addition, the effect of the value of transport resistance was assessed by varying the groundwater transit time.

The main difference in the approaches of TILA-99 and the present study is the use of

- a numerical model with two finite domains with different rock parameter values in TILA-99 and
- an analytical model with one infinite and homogenous domain with single rock parameter values in the present study.

The differences of the results of these models can to a large extent be explained by this main difference in the modelling approaches. In addition, the results of the present study are also similar to those presented in TILA-99. Consequently, the results presented in TILA-99 are confirmed, i.e., they are such as they can be expected to be with the kind of a model that has been used. As a consequence, the conclusions made in TILA-99 [1, p. 145] hold. I.e., the geosphere is an efficient transport barrier for well-sorbing nuclides and for short-lived nuclides and a poor barrier for non-sorbing nuclides.

In TILA-99, the effects of the rock characteristics have been studied by means of varying the rock depth accessible for the matrix diffusion. Limiting of the penetration depth has not affected much the release rates of the non-sorbing or the strongly-sorbing elements. Some effect has been found on the moderately-sorbing nuclides so that the maximum dose rates in the very high flow scenarios have been increased at most by a factor of about two when matrix diffusion is restricted only to the first centimetre of altered rock adjacent to the water-conducting fracture [1, p. 165].

In addition to this information on rock characteristics obtained in TILA-99, the effect of the rock parameter values is found to be significant for some cases in the present study. E.g., for Ni-59 in DC-ns50 and for Sr-90 in SH-sal50 scenario, the maximum release rates are changed by more than a factor of $10^2$ and $10^4$, respectively, if the rock parameter values of the intact rock zone and the zone of altered rock adjacent to the fracture are interchanged.

Variation of the transport resistance by varying the value of the groundwater transit time affects the result in some cases considerably, though the shapes of the results are not changed. The results are the most sensitive for the nuclides that have a small half life compared to the transit time. According to VTT, the simple model is the least applicable to these cases [12].

Assumptions of the model were the following:

- The fracture is long, thin, smooth, and rigid with stationary characteristics.
- The fracture and the porous rock are saturated.
- The groundwater velocity in the fracture is constant and directed one-dimensionally along the fracture.

- Water and rock characteristics do not depend on position.
- The concentration in the fracture fluid is independent of the position in the direction perpendicular to the fracture axis.
- Transport in the porous rock occurs slowly and one-dimensionally by molecular diffusion in the direction perpendicular to the fracture axis.
- Decay chains are not taken into account; the model is for a single nuclide.
- The retardation on the inner surfaces of the porous rock is modelled by assuming the nuclides to spend a given fraction of the time in immobile phase.

Varying of the transit time had in some cases a significant effect on the result. Decreasing the transit time too much is unrealistic, because actual groundwater velocities are not very large. On the other hand, increasing the transit time conflicts with the model assumptions. When the transit time is increased, velocity of the water in the fracture is not much larger than in the rock matrix any more, penetration depths are increased and the transport can no longer be expected to be one-dimensional in either the direction of the fracture or in the direction of the matrix.

Modelling natural phenomena, like the groundwater flow in rock, involves large uncertainties in the actual nature of the phenomena as well as in the values of the appropriate parameters. Some of the main differences between the transport model used and the reality are the mathematical characterisation of the flow route in rock as a smooth and straight fracture and the modelling of the complicated chemical processes causing retardation with the help of a distribution coefficient that does not explain those phenomena.

The reason why this kind of an overly simplified deterministic physical model can be used in such a case is the assumption of conservatism. The model is supposed to represent the worst possible realistic situation. The model does not represent the actual situation well but using it provides understanding of the key characteristics involved. The model is simple and 'robust' with few parameters, the effects of which are clearly visible and the inclusion of which is justified.

On the other hand, even the most advanced and sophisticated models are only simplified ways to describe the phenomena for which the models are created. Nevertheless, such models can be so complex, that the effects of individual phenomena incorporated can not be assessed by using them. Such approaches do not necessarily give any new information on the problem to be studied.

# REFERENCES


[1] T. Vieno, H. Nordman: *Safety assessment of spent fuel disposal in Hästholmen, Kivetty, Olkiluoto and Romuvaara. TILA-99.* POSIVA-99-07, Posiva Oy, Helsinki 1999.

[2] T. Vieno, A. Hautojärvi, L. Koskinen, H. Nordman: *TVO-92 Safety analysis of spent fuel disposal*. Report YJT-92-33 E, Nuclear Waste Commission of Finnish Power Companies, Helsinki 1993.

[3] A. Hautojärvi: *Matriisidiffuusion vaikutus rakokulkeutumisessa.* Helsinki, Valtion teknillinen tutkimuskeskus, Ydinvoimatekniikan laboratorio, Työraportti TOKA-4/89. (In Finnish)

[4] H.S. Carslaw, J.C. Jaeger: *Conduction of Heat in Solids*. Second edition, Clarendon Press, Oxford, 1995.

[5] D.H. Tang, E.O. Frind, E.A. Sudicky: *Contaminant Transport in Fractured Porous Media: Analytical Solution for a Single Fracture*. Water Resources Research, Vol. 17, No. 3, Pages 555–564, June 1981.

[6] M. Elert: *Retention mechanisms and the flow wetted surface - implications for safety analysis.* SKB TR 97-01, Swedish Nuclear Fuel and Waste Management Co, February 1997.

[7] F.P. Incropera, D.P. de Witt: *Fundamentals of Heat and Mass Transfer*. Second edition, John Wiley & Sons, Inc. Singapore, 1985.

[8] K. Rasilainen, A. Luukkonen, A. Niemi, M. Olin, J. Pöllä: *The feasibility of modelling coupled processes in safety analysis of spent nuclear fuel disposal.* Research Notes 1973, Technical Research Centre of Finland, Libella Painopalvelu Oy, Espoo, 1999.

[9] K. Rasilainen: *Radionuklidien kulkeutumistarkastelut käytetyn ydinpolttoaineen sijoituspaikkatutkimusten suunnittelussa.* Lisensiaattityö, Teknillinen korkeakoulu, Tietotekniikan osasto, Teknillisen fysiikan laitos, Espoo, 1987. (In Finnish)

[10] E.A. Sudicky, E.O. Frind: *Contaminant Transport in Fractured Porous Media: analytical solutions for two-member decay-chain in a single fracture.* Water Resources Research, Vol. 20, No. 7, Pages 1021-1029, 1984.

[11] E. Kreyszig: *Advanced Engineering Mathematics*. Seventh edition. John Wiley & Sons, Inc., United States, 1993.

[12] T. Vieno, H. Nordman. VTT Energy. Interview, September 1999.

[13] FTRANS. *A two-dimensional code for simulating fluid flow and transport of radioactive nuclides in fractured rock for repository performance assessment.* Intera Environmental Consultants Inc., Report ONWI-426, Houston, 1983.

[14] T. Vieno, H. Nordman. VTT Energy. E-mail correspondence, August 1999.

[15] T. Vieno. VTT Energy. E-mail correspondence, November 1999.

## APPENDIX 1 ELEMENTARY LAPLACE TRANSFORMATION

Laplace transformation [11, p. 317] with respect to time is defined as

$$L\{g(\mathbf{r},t)\} = \bar{g}(\mathbf{r},p) = \int_0^\infty e^{-pt} g(\mathbf{r},t)\,dt \tag{A.1}$$

where

$L$ is the Laplace transformation operator,
$g$ is an arbitrary function of position and time,
$\bar{g}$ is the Laplace transform of the same function,
$p$ is the Laplace variable.

Transform of a derivative of a function is

$$L\left\{\frac{dg(\mathbf{r},t)}{dt}\right\} = p\bar{g}(\mathbf{r},p) - g_0, \tag{A.2}$$

where

$$g_0 = g(\mathbf{r},t=0). \tag{A.3}$$

Multiplication of a transform by an exponential function leads to $t$-shifting:

$$L^{-1}\left\{e^{-t_0 p}\bar{g}(\mathbf{r},p)\right\} = U(t-t_0)\,g(\mathbf{r},t-t_0), \tag{A.4}$$

where

$L^{-1}$ is the Laplace inverse transformation operator,
$t_0$ is a fixed time point (s) and
$U$ is the Heaviside unit step function for which [11, p. 278]

$$\begin{aligned} U(t-t_0) &= 0, \quad t < t_0, \\ U(t-t_0) &= 1, \quad t > t_0. \end{aligned} \tag{A.5}$$

Change of the Laplace variable leads to $p$-shifting:

$$L^{-1}\left\{\bar{g}(\mathbf{r},p+\lambda)\right\} = e^{-\lambda t} g(\mathbf{r},t). \tag{A.6}$$

## DERIVATION OF THE SOLUTION OF 1D MODEL WITH $D_f = 0$ — APPENDIX 2

By performing a Laplace transformation (A.1, A.3, A.4) on (59–65) with $D_f$ =0, we get the subsidiary problem

$$\frac{\partial \overline{C}_f(x,p)}{\partial x} = -\frac{R_f}{v}(p+\lambda)\overline{C}_f(x,p) + \frac{R_f}{v}\frac{2}{2b}\frac{\varepsilon D_p}{R_f}\frac{\partial \overline{C}_p(x,z,p)}{\partial z}\bigg|_{|z|=b}; \quad |z| = b, \tag{A.7}$$

$$\frac{\partial^2 \overline{C}_p(x,z,p)}{\partial z^2} = \frac{R_p}{D_p}(p+\lambda)\overline{C}_p(x,z,p), \quad |z| \geq b, \tag{A.8}$$

$$\overline{C}_f(x,p) = \overline{C}_p(x,z,p); \quad |z| = b, \tag{A.9}$$

$$\overline{C}_f(x=0,p) = C_0/p, \tag{A.10}$$

$$\lim_{x\to\infty} \overline{C}_f(x,p) = 0, \tag{A.11}$$

$$\lim_{z\to\pm\infty} \overline{C}_p(x,z,p) = 0. \tag{A.12}$$

With the condition (A.12), the solution of (A.8) in the different ranges is

$$\begin{aligned} \overline{C}_p(x,z,p) &= C^1(x,p)e^{-B\sqrt{p+\lambda}z}, \quad z \geq b, \\ \overline{C}_p(x,z,p) &= C^2(x,p)e^{B\sqrt{p+\lambda}z}, \quad z \leq -b, \end{aligned} \tag{A.13}$$

where

$C^1$ and $C^2$ are constants (which do not depend on $z$)

and $B$ is as in (76). With the help of the boundary condition (A.9), (A.13) can be stated in the form

$$\overline{C}_p(x,z,p) = \overline{C}_f(x,p)e^{-B\sqrt{p+\lambda}(|z|-b)}, \quad |z| \geq b. \tag{A.14}$$

For (A.7), we need the derivative of $C_p$ at $|z| = b$, which from (A.14) is

$$\frac{\partial \overline{C}_p(x,z,p)}{\partial z}\bigg|_{|z|=b} = -B\sqrt{p+\lambda}\,\overline{C}_f(x,p), \quad |z| = b. \tag{A.15}$$

From (A.7, A.15), the subsidiary equation for the fracture becomes

$$\begin{aligned} \frac{\partial \overline{C}_f(x,p)}{\partial x} &= -\frac{R_f}{v}(p+\lambda)\overline{C}_f(x,p) - \frac{R_f}{v}\frac{2}{2b}\frac{\varepsilon D_p}{R_f}B\sqrt{p+\lambda}\,\overline{C}_f(x,p) \\ &= -\frac{R_f}{v}\left(p+\lambda+\frac{2}{2b}\frac{\varepsilon D_p}{R_f}B\sqrt{p+\lambda}\right)\overline{C}_f(x,p) \\ &= -\frac{R_f}{v}\left(P+\frac{\sqrt{P}}{A}\right)\overline{C}_f(x,p) \quad , \end{aligned} \tag{A.16}$$

## APPENDIX 2 DERIVATION OF THE SOLUTION OF 1D MODEL WITH $D_f = 0$

where $A$ and $B$ are abbreviations defined in (75) and (76), respectively. $P$ is defined as

$$P = p + \lambda . \tag{A.17}$$

The solution of (A.16) is

$$\overline{C}_f(x, p) = C^3(p) e^{-\frac{R_f}{v}\left(P + \frac{\sqrt{P}}{A}\right)x}, \tag{A.18}$$

where

$C^3$ is a constant (which does not depend on $x$).

By the inlet condition (A.10) the subsidiary solution (A.18) for the fracture becomes

$$\overline{C}_f(x, p) = \frac{C_0}{p} e^{-\frac{R_f}{v}\left(P + \frac{\sqrt{P}}{A}\right)x}. \tag{A.19}$$

By substituting (A.19) to (A.14), we get the subsidiary solution for the matrix to be

$$\overline{C}_p(x, z, p) = \frac{C_0}{p} e^{-\frac{R_f}{v}\left(P + \frac{\sqrt{P}}{A}\right)x - B\sqrt{P}(|z| - b)}, \quad |z| \geq b. \tag{A.20}$$

To inverse transform (A.19, A.20), we make use of the identity found in [4, APP V, eq.19]

$$L^{-1}\left\{\frac{e^{-\frac{x}{\sqrt{\kappa}}\sqrt{p}}}{p - \alpha}\right\} = \frac{1}{2} e^{\alpha t}\left[e^{-\sqrt{\frac{\alpha}{\kappa}}x} \operatorname{erfc}\left(\frac{x}{2\sqrt{\kappa t}} - \sqrt{\alpha t}\right) + e^{\sqrt{\frac{\alpha}{\kappa}}x} \operatorname{erfc}\left(\frac{x}{2\sqrt{\kappa t}} + \sqrt{\alpha t}\right)\right] \tag{A.21}$$

where

$\alpha$ is a constant,

$\kappa$ is the diffusivity (m²/s) as defined in (6), but here treated as a constant.

By (A.17) and by rearrangement of terms, the subsidiary solutions (A.19, A.20) can be written in the form

$$\frac{\overline{C}_f(x, P)}{C_0} = e^{-t_0 P} \frac{e^{-\frac{t_0}{A}\sqrt{P}}}{P - \lambda}, \tag{A.22}$$

$$\frac{\overline{C}_p(x, z, P)}{C_0} = e^{-t_0 P} \frac{e^{-Z\sqrt{P}}}{P - \lambda}, \tag{A.23}$$

where

$$t_0 = \frac{R_f}{v} x, \tag{A.24}$$

$$Z = \frac{R_f}{vA} x + B(|z| - b) = \frac{t_0}{A} + B(|z| - b). \tag{A.25}$$

## DERIVATION OF THE SOLUTION OF 1D MODEL WITH $D_f = 0$ — APPENDIX 2

From (A.4, A.6, A.17) it follows

$$L^{-1}\left\{e^{-t_0 P}\,\overline{g}(\mathbf{r},P)\right\} = e^{-\lambda t}\,g(\mathbf{r},t-t_0)\cdot U(t-t_0), \tag{A.26}$$

and from (A.21, A.26) the inverse transforms of (A.22, A.23) are

$$\begin{aligned}
&\frac{C_f(x,t)}{C_0} = 0, \quad t < t_0,\\
&\frac{C_f(x,t)}{C_0} = \frac{1}{2}e^{-\lambda t_0}\left[e^{-\frac{\sqrt{\lambda}t_o}{A}}\operatorname{erfc}\left(\frac{t_0}{2A\sqrt{t-t_0}} - \sqrt{\lambda(t-t_0)}\right) + \right.\\
&\qquad\left. + e^{\frac{\sqrt{\lambda}t_o}{A}}\operatorname{erfc}\left(\frac{t_0}{2A\sqrt{t-t_0}} + \sqrt{\lambda(t-t_0)}\right)\right], \quad t > t_0,
\end{aligned} \tag{A.27}$$

$$\begin{aligned}
&\frac{C_p(x,z,t)}{C_0} = 0, \quad t < t_0,\\
&\frac{C_p(x,z,t)}{C_0} = \frac{1}{2}e^{-\lambda t_0}\left[e^{-\sqrt{\lambda}Z}\operatorname{erfc}\left(\frac{Z}{2\sqrt{t-t_0}} - \sqrt{\lambda(t-t_0)}\right) + \right.\\
&\qquad\left. + e^{\sqrt{\lambda}Z}\operatorname{erfc}\left(\frac{Z}{2\sqrt{t-t_0}} + \sqrt{\lambda(t-t_0)}\right)\right], \quad t > t_0.
\end{aligned} \tag{A.28}$$

## APPENDIX 3 RELEASE RATES OF ACTIVATION PRODUCTS IN SH-SAL50 SCENARIO

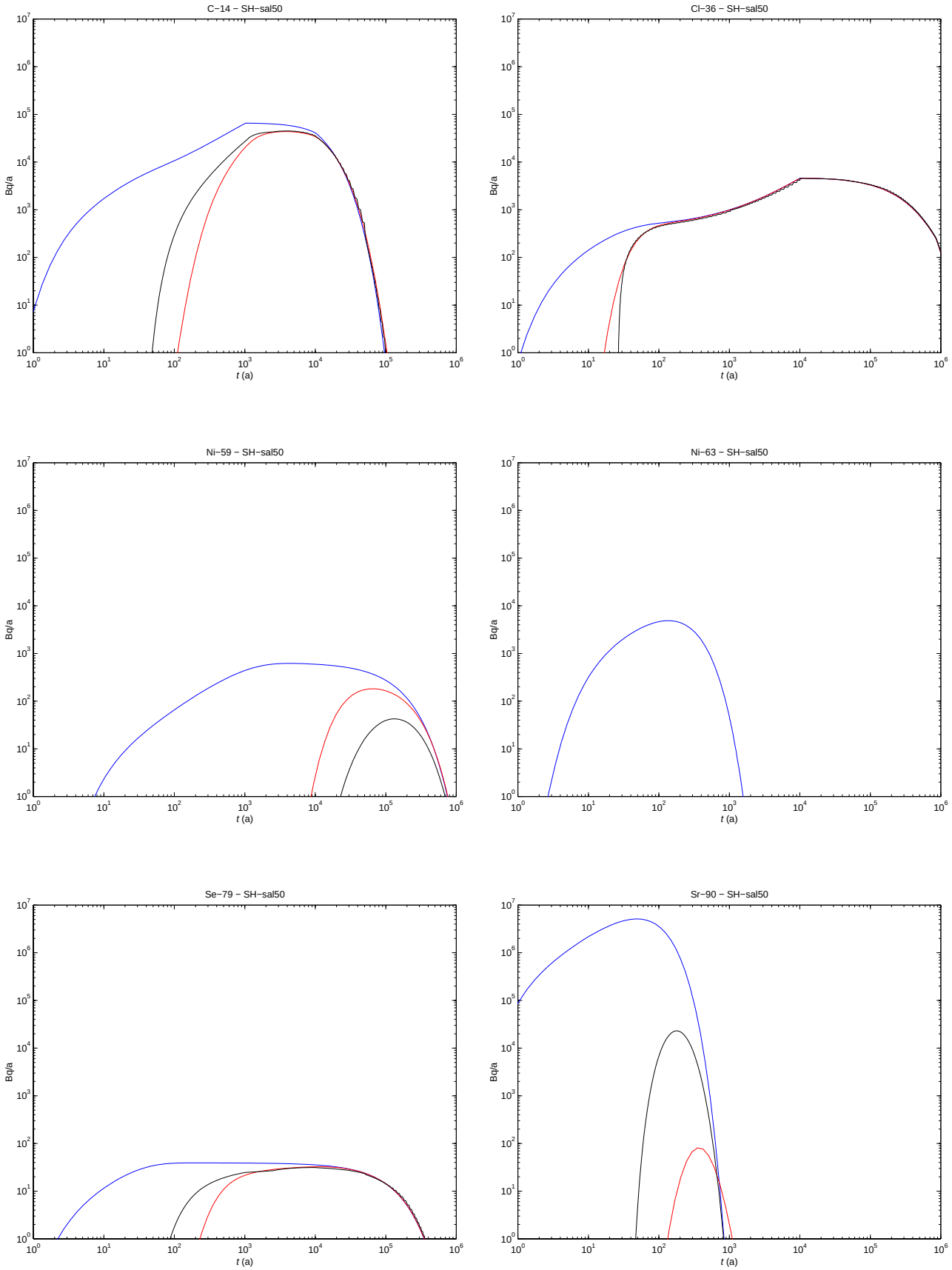


***Blue**: TILA-99-input; **Red**: TILA-99-output; **Black**: Result output of the present study*

RELEASE RATES OF FISSION PRODUCTS IN SH-SAL50 SCENARIO

**APPENDIX 4**

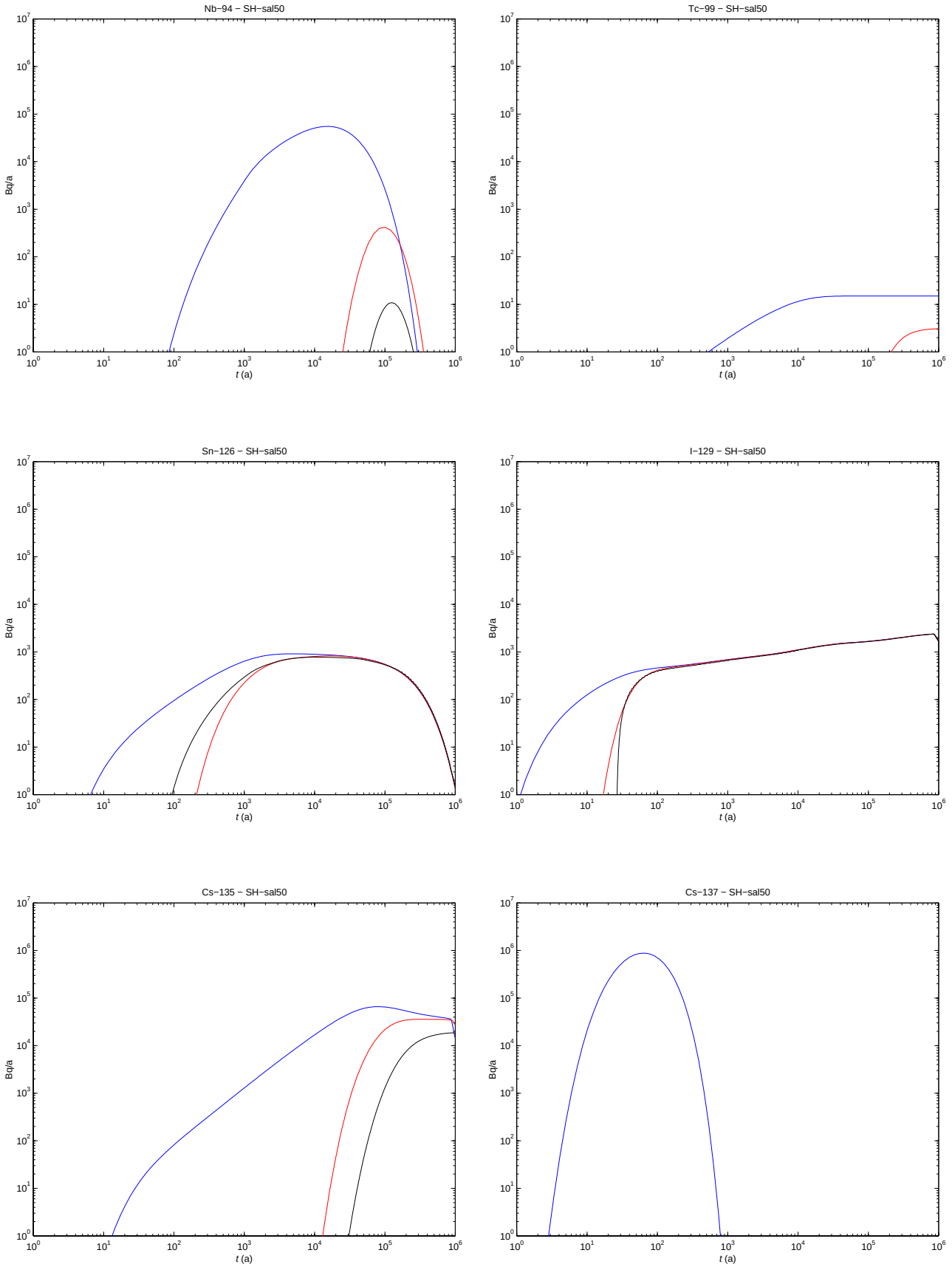


***Blue**: TILA-99-input; **Red**: TILA-99-output; **Black**: Result output of the present study*

## APPENDIX 5 RELEASE RATES OF ACTIVATION PRODUCTS IN DC-NS50 SCENARIO

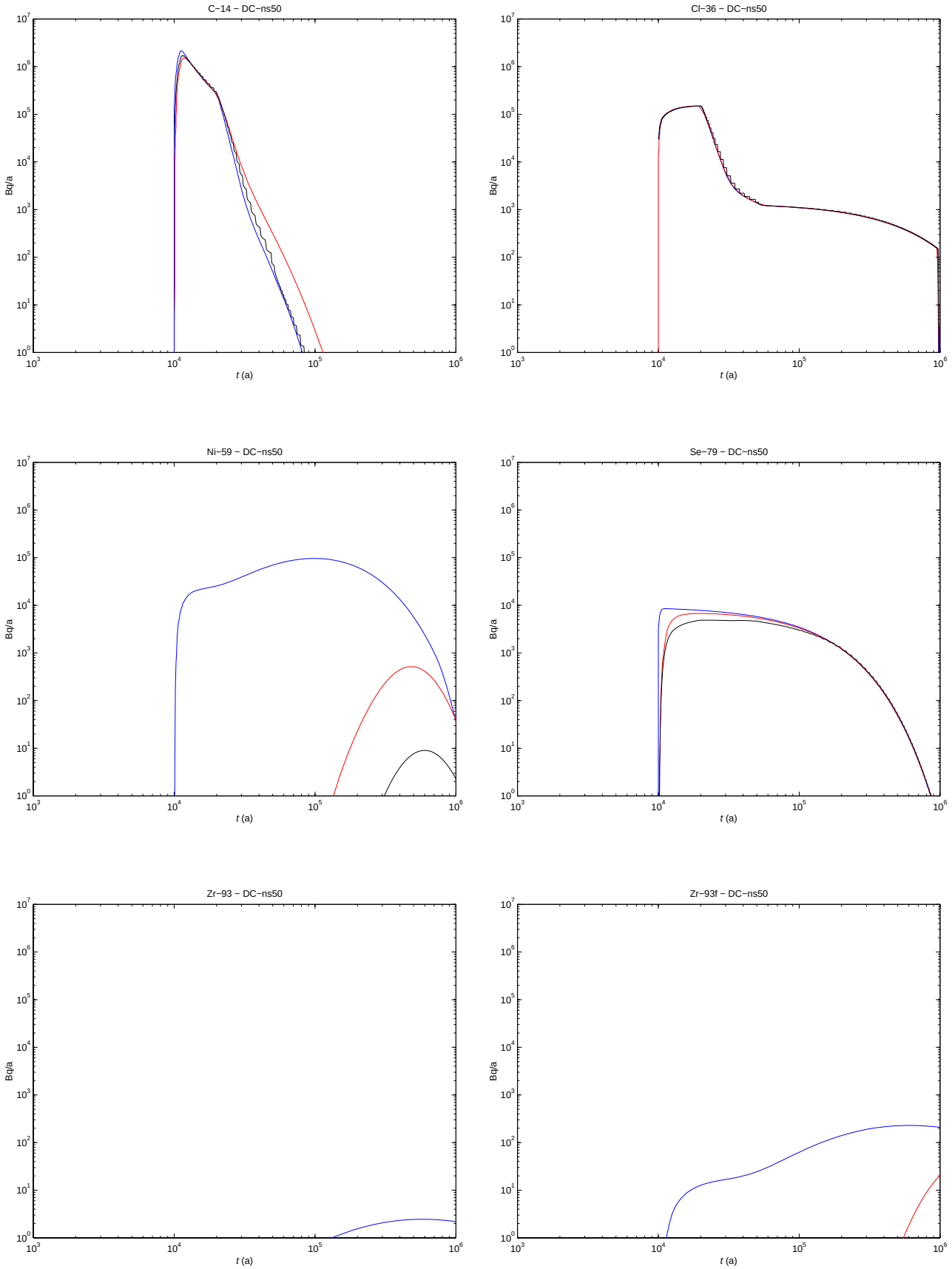


***Blue**: TILA-99-input; **Red**: TILA-99-output; **Black**: Result output of the present study*

RELEASE RATES OF FISSION PRODUCTS IN DC-NS50 SCENARIO

**APPENDIX 6**

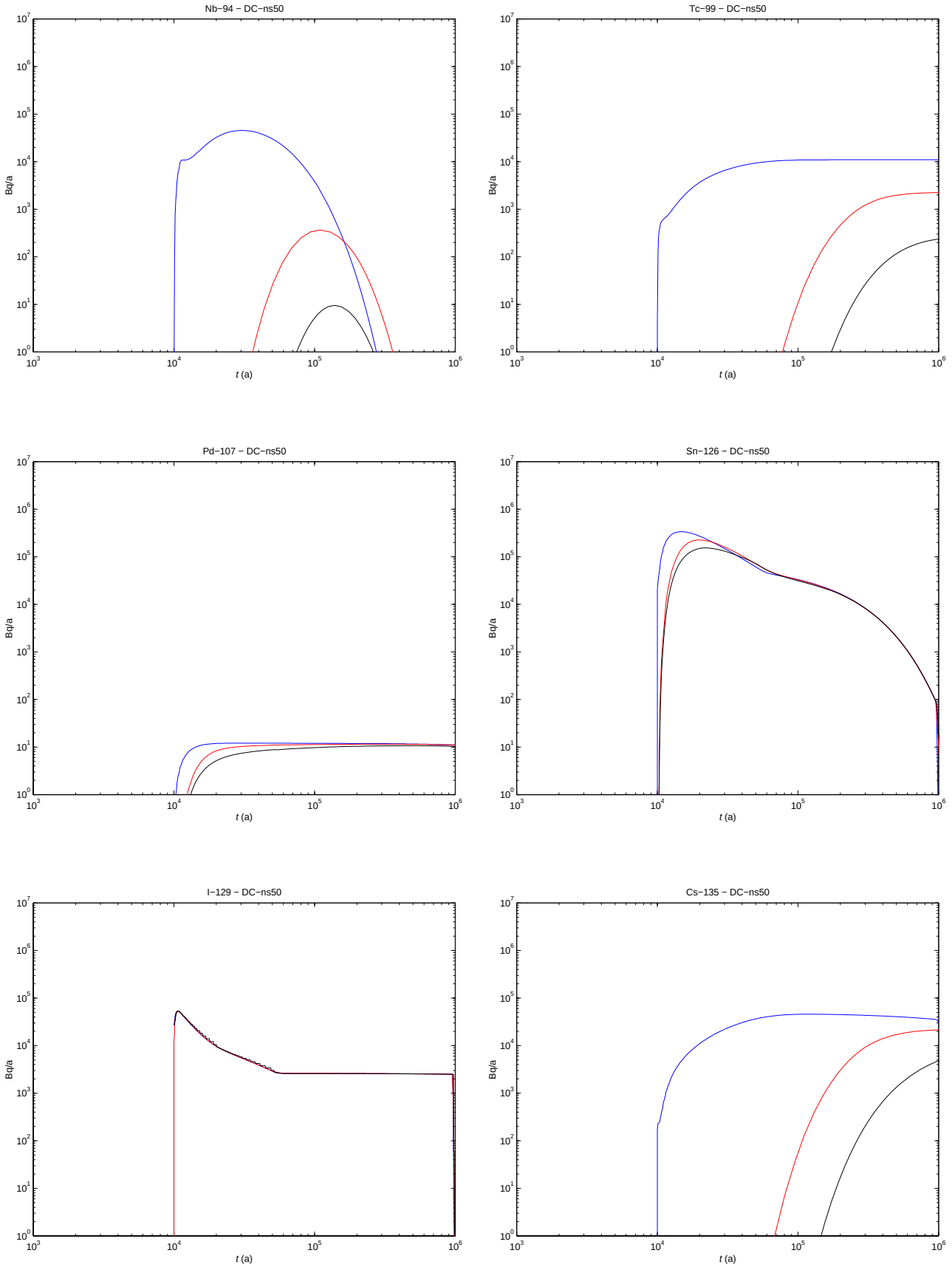


***Blue**: TILA-99-input; **Red**: TILA-99-output; **Black**: Result output of the present study*

## APPENDIX 7

SMALL RELEASE RATES IN SH-SAL50 AND DC-NS50 SCENARIOS

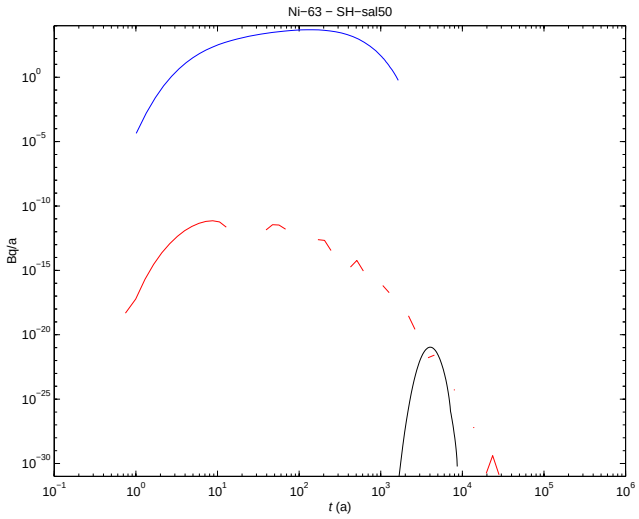


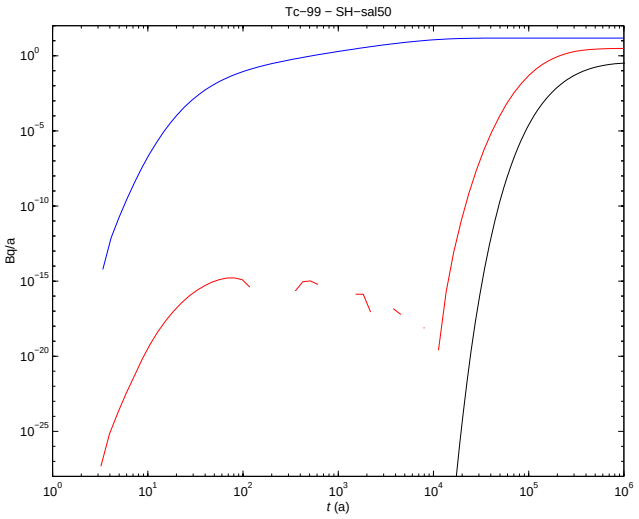


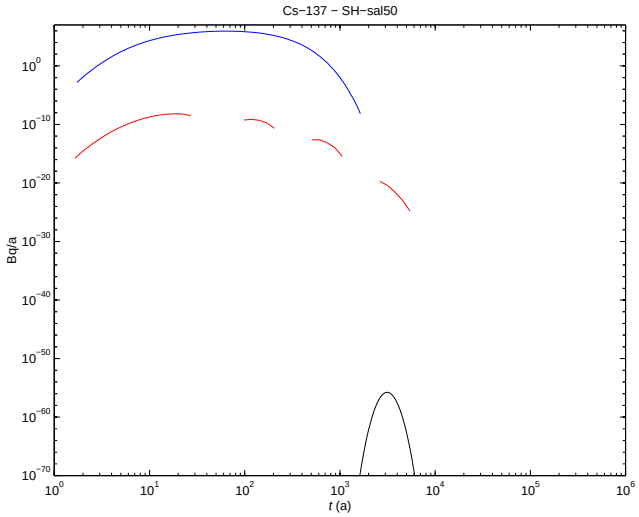


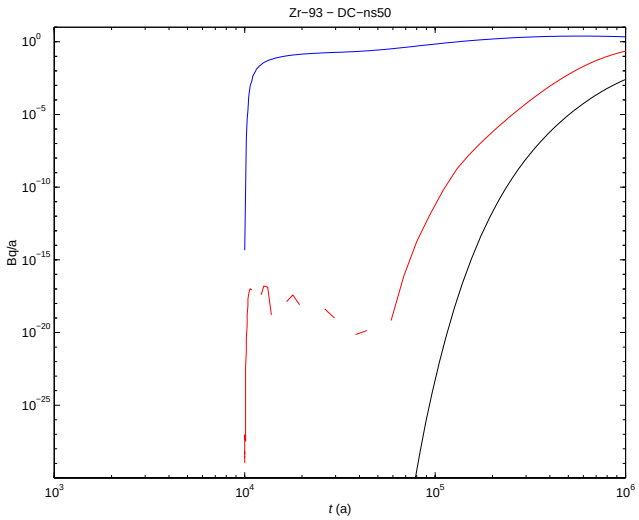


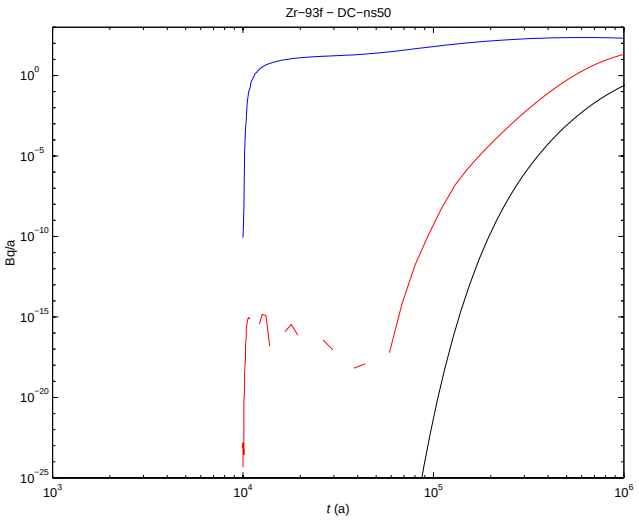


***Blue**: TILA-99-input; **Red**: TILA-99-output; **Black**: Result output of the present study*

THE CALCULATION PROGRAM

# APPENDIX 8

The input data with the time and the release rate vectors in their respective columns are found in .dat files for each scenario and nuclide. An additional datum is the size of the data file, i.e., the length of both the columns. The data files are not presented here, but the data are plotted in main report's Figures 4 and 5.

*Beginning of an exemplary input data file*

```
169
0.00E+00            1.22E-09
2.75E-01            2.38E-04
4.80E-01            6.29E-02
7.22E-01            1.24E+00
1.01E+00            7.86E+00
1.34E+00            2.76E+01
.                   .
.                   .
.                   .
```

The program consists of four parts:

1. **actual.m** is the main script that does the following:
- takes the names of the nuclide and the scenario as inputs from the keyboard
- calls the function input.m to get the corresponding TILA-99 input and output vectors and the time vectors
- calls the function params.m to get the given nuclide and scenario specific parameter values
- calculates derived parameters on the basis of the given parameters
- forms the calculation lattice for each individual rectangular pulse by making the vector DT denser and shifting it by t0 ($t_0$)
- in a calculation loop:
  - calls the function C_out.m for each individual rectangular pulse
  - assigns the output for each individual pulse in the correct portion of the calculation lattice
  - adds the outputs of the individual pulses to the result output vector
  - when needed, plots the outputs of the individual pulses
- plots the result output in $\log_{10}$–$\log_{10}$ scale
- displays
  - the values of the parameters used
  - the maximum release rate and the time of its occurrence
  - calculation time used

2. **input.m** is a function that does the following:
- takes the names of the nuclide and the scenario as inputs
- reads the corresponding TILA-99 input data from a .dat file
- forms the corresponding time vector T_in and the release rate vector C_in and the vector of time differences DT_in
- reads the corresponding TILA-99 output data from a .dat file
- forms the corresponding time vector T_out and the release rate vector C_out
- plots the TILA-99 input and output in $\log_{10}$–$\log_{10}$ scale
- gives the TILA-99 input release rate C_in, width of each individual rectangular input pulse DT_in, and the time vector T_in as outputs

3. **params.m** is a function that does the following:
- takes the names of the nuclide and the scenario as inputs
- assigns the case specific information
  - determines the salinity condition according to the scenario
  - determines the chemical status: Y = anion, N = non-anion
  - determines the $K_d$ value according to the salinity condition
  - determines the values of the rock parameters e_p ($\varepsilon$) and D_e ($D_e$) according to the K_d ($K_d$) value
  - determines the half life T_half ($T_{½}$) of the nuclide
- gives nuclide and scenario specific e_p, D_e, K_d, K_a, and T_half as an output ($K_a$ = K_a = 0)

4. **C_out.m** is a function that does the following:
- takes the given and the derived parameter values and the appropriate portion of the calculation lattice as inputs
- calculates an output of an individual rectangular pulse as a difference of the outputs of two step functions shifted by DT
- when needed, removes possible unphysical negative values from the output
- gives the output of an individual rectangular pulse as an output

```
% ------------------------------------------------------------
% REVIEW OF TILA-99 RESULTS - MAIN PROGRAM
% ------------------------------------------------------------
% Summation of individual outputs of rectangular inputs on the
% basis of an analytical solution for a constant inlet condition.
% TILA-99 results in Figures 11-5, p. 137 and 11-9, p. 141.
% ------------------------------------------------------------
% Parameters      TILA-99
% ---------------------------------------
% WL/Q:     p.132 and Table 11-19, p.133;
% e_p, D_e: Table 11-10, p. 120;
% K_d:      Table 11-9, p.118;
% T_half:   Table 2-3, p.21;
% ------------------------------------------------------------
% Last modification 9.11.99
% ------------------------------------------------------------

clc, clear

% calculation lattice parameters
% coeff = 20; N_DTi = 2; % SH-sal50: C-14, Se-79, Sr-90, Sn-126
                         % DC-ns50:  Se-79,
% coeff = 20; N_DTi = 5; % DC-ns50: C-14
% coeff = 10; N_DTi = 4; % SH-sal50: Cl-36, I-129
% coeff = 70; N_DTi = 1; % SH-sal50: Ni-59, Ni-63, Nb-94, Tc-99, Cs-135, Cs-137
                         % DC-ns50:  Ni-59, Zr-93, Nb-94, Tc-99, Cs-135
% coeff = 30; N_DTi = 1; % DC-ns50: Pd-107
% coeff = 50; N_DTi = 1; % DC-ns50: Cl-36
                         % DC-ns50: Sn-126
% coeff = 3; N_DTi = 5;  % DC-ns50: I-129

% ------------------------------------------------------------
% Choice of the nuclide and the scenario interactively.
% ------------------------------------------------------------

fprintf('List of the nuclides:\n\n');
fprintf('C-14  Cl-36  Cs-135 Cs-137 I-129 Nb-94 Ni-59\n');
fprintf('Ni-63 Pd-107 Se-79  Sn-126 Sr-90 Tc-99 Zr-93 Zr-93f\n\n');

% the name of the nuclide
nucl = input('Enter the name of the nuclide : ','s');

fprintf('List of the scenarios:\n\n');
fprintf('SH-sal50 DC-ns50\n\n');

scen = input('Enter the scenario : ','s');
% ------------------------------------------------------------

t=cputime;  % Execution starting point

% ------------------------------------------------------------
% Input data according to the nuclide and the scenario
% RECTANGULAR PULSE:
% The size of a pulse (C0, DT):
% C0 = Height = discrete input values
% DT = Width = durations of individual pulses

[T0, DT, C0] = input(nucl, scen);
% ------------------------------------------------------------


% ------------------------------------------------------------
% PARAMETERS - Given and Derived
% ------------------------------------------------------------

% -------------------------------------------------------
% Given parameters
% rho, WL/Q, D_e, e_p, K_d, K_a, T_half,
% -------------------------------------------------------
```

```
% The given parameters according to the nuclide and the scenario
[e_p, D_e, K_d, K_a, T_half] = params(nucl, scen);

% The given constant parameter
rho = 2700; % rock density (kg/m^3)

% The given transport resistance parameter
% WL/Q: BASE CASE ("50") (TILA-99, p.132 and Table 11-19):
% Transport resistance 5*10^4 a/m can be illustrated to be
% WL/Q = t_w/2b = 25a/5*10^-4m = 5*10^4 a/m
% WL/Q = (0.1 m * 600 m)/1.2 l/a = 5*10^4 a/m
t_w = 25;         % Transit time (a)

b2 = 5d-4;        % (2bv) volume aperture (m)


% ------------------------------------------------------------
% Derived parameters
% D_p, R_f, R_p, lambda
% ------------------------------------------------------------

D_p = D_e/e_p;               % eq. (85)
R_p = 1+K_d*rho*(1-e_p)/e_p; % eq. (27)
R_f = 1+2*K_a/b2;            % eq. (23)
lambda = log(2)/T_half;

% ------------------------------------------------------------
% Auxiliary parameters
% ------------------------------------------------------------

A = (b2/2)*R_f/(e_p*sqrt(R_p*D_p));      % eq. (75)
t0 = t_w*R_f; % t0 = t_w*R_f = (x/v)*R_f % eq. (79)

% ------------------------------------------------------------
% CALCULATIONS AND PLOTS
% ------------------------------------------------------------

% Division of each DT(i) in N_DTi parts
% => denser lattice TS: length(TS) = N_DTi*length(DT)

N_DT = length(DT);

TS = zeros(0); % initialization, an empty matrix
Tf = T0(N_DT); % initialization of the end of the "regular" TS

extension = 10;

for i = 1:N_DT+coeff+extension
   if i < N_DT
      TSi = [T0(i)+DT(i)/N_DTi:DT(i)/N_DTi:T0(i)+DT(i)];
      TS = [TS TSi];
   else
      TSi = [Tf+DT(N_DT)/N_DTi:DT(N_DT)/N_DTi:Tf+DT(N_DT)];
      TS = [TS TSi];
      Tf = Tf + DT(N_DT);
   end
end

CL = TS+t0; % The Calculation Lattice

N_CS = length(TS);
CS = zeros(1, N_CS); % initialization of the result vector CS

for i = 1:N_DT
   fprintf('%d/%0.5g\n', i, N_DT);
   T = CL((i-1)*N_DTi+1:(i-1)*N_DTi+coeff*N_DTi) - T0(i);
   C = C_out802(A, t0, lambda, R_f, C0(i), DT(i), T, N_DTi);
```

## APPENDIX 9 1/4 THE CODE

```
   Cs = zeros(1, N_CS); % initialization of an individual output
   Cs((i-1)*N_DTi+1:(i-1)*N_DTi+coeff*N_DTi) = C;

   CS = CS + Cs;  % The result is the sum of the individual output pulses.
%  figure(1), hold on   % an option to plot the individual outputs
%  loglog(CL, Cs)
end

figure(1), hold on
loglog(CL, CS,'k-')

xlabel('\itt\rm (a)');ylabel('Bq/a');
title(['',sprintf(nucl),' - ',sprintf(scen)])
% ------------------------------------------------------------

D_e1 = D_e/(365*24*3600); % unit conversion [D_e] = (m^2/s)
[maxCS, max_i] = max(CS);
max_CL = CL(max_i);

fprintf('------------------\n');
fprintf('End of calculation\n');
fprintf('------------------\n');
fprintf('\n[e_p, D_e, K_d, K_a, T_half]=');
fprintf('%0.5g %0.5g %0.5g %0.5g %0.5g\n', e_p, D_e1, K_d, K_a, T_half);
fprintf('\nMaximum release = %0.2g Bq/a at t = %0.2g a\n', maxCS, CL(max_i));

time_elapsed = cputime-t;     % Execution final point
fprintf('\nCalculation time %0.3g s\n', time_elapsed);
```

```
% ------------------------------------------------------------
% Loading and visualisation of data received from VTT.
% Formation of the data vectors T, C0 and DT
% ------------------------------------------------------------
% Last modification 9.11.99
% ------------------------------------------------------------

function [T0_in, DT_in, C0_in] = input(nucl, scen)

% ------------------------------------------------------------
% Given input data
% ------------------------------------------------------------

% Reading the name of the nuclide and the size of the data vectors.

% E.g. for nuclide C-14 and scenario SH-sal50, the name of the file
% containing the VTT-input data is data/C-14_in_SH-sal50.dat

file = sprintf('data/%s_in_%s.dat', nucl, scen);
fid_in = fopen(file,'r'); % read the size and the data

nuc_size_in = fread(fid_in, 3); % read the size
s_in = setstr(nuc_size_in');
size_in = sscanf(s_in,'%i'); % size of the data vectors (an int)

inp_in_1 = fscanf(fid_in,'%g',[2 size_in]); % read the data
inp_in_2 = inp_in_1';
T0_in = inp_in_2(:,1);  % time is in the first column
DT_in = diff(T0_in);    % lengths of the pulses as differences
C0_in = inp_in_2(:,2);  % heights of the pulses are in the 2. column
status = fclose(fid_in);     % closing the file

% Length of DT is reduced when differencing => equalisation
C0_in = C0_in(1:size_in-1); % length(DT) = length(T0)-1
T0_in = T0_in(1:size_in-1); % length(DT) = length(T0)-1
% ------------------------------------------------------------

% ------------------------------------------------------------
% Given output data
% ------------------------------------------------------------

% Reading the name of the nuclide and the size of the data vectors.

% E.g. for nuclide C-14 and scenario SH-sal50, the name of the file
% containing the VTT-output data is data/C-14_out_SH-sal50.dat

file = sprintf('data/%s_out_%s.dat', nucl, scen);
fid_out = fopen(file,'r'); % read the size and the data

nuc_size_out = fread(fid_out, 3); % read the size
s_out = setstr(nuc_size_out');
size_out = sscanf(s_out,'%i'); % size of the data vectors (an int)

inp_out_1 = fscanf(fid_out,'%g',[2 size_out]); % read the data
inp_out_2 = inp_out_1';
T0_out = inp_out_2(:,1);     % time is in the first column
C0_out = inp_out_2(:,2);     % heights of the pulses are in the 2. column
status = fclose(fid_out);    % closing the file

% ------------------------------------------------------------
% Plots
% ------------------------------------------------------------

figure(1), clf, loglog(T0_in, C0_in,'b-');
figure(1), hold on, loglog(T0_out, C0_out,'r-');
axis([1d+0 1d+6 1d+0 1d+7]);
```

```
% ------------------------------------------------------------
% Given nuclide dependent parameter values
% e_p, D_e, K_d, K_a, T_half
% ------------------------------------------------------------
% Last modification 9.11.99
% ------------------------------------------------------------

function [e_p, D_e, K_d, K_a, T_half] = params(nucl, scen)

% ------------------------------------------------------------
% each salinity condition is assigned an arbitrary number

while length(scen) < 8
   scen = sprintf('%s ', scen);
end

if scen == 'DC-ns50 '
      sal = 1;    % non-saline
elseif scen == 'SH-sal50'
      sal = 2;    % saline
end
% ------------------------------------------------------------
% Each nuclide is assigned a number in alphabetical order
% C-14 C-36 Cs-135 Cs-137 I-129 Nb-94 Ni-59 Ni-63 Pd-107 Se-79
% Sn-126 Sr-90 Tc-99 Zr-93
%
% and an indicator 'anion':
% anion = 'Y' => anion; anion = 'N' => non-anion
% TILA-99, TABLE 11-10, p. 120

while length(nucl) < 6
   nucl = sprintf('%s ', nucl);
end

if nucl == 'C-14  '
      n = 1; anion = 'Y';
elseif nucl == 'Cl-36 '
      n = 2; anion = 'Y';
elseif nucl == 'Cs-135'
      n = 3; anion = 'N';
elseif nucl == 'Cs-137'
      n = 4; anion = 'N';
elseif nucl == 'I-129 '
      n = 5; anion = 'Y';
elseif nucl == 'Nb-94 '
      n = 6; anion = 'N';
elseif nucl == 'Ni-59 '
      n = 7; anion = 'N';
elseif nucl == 'Ni-63 '
      n = 8; anion = 'N';
elseif nucl == 'Pd-107'
      n = 9; anion = 'Y';
elseif nucl == 'Se-79 '
      n = 10; anion = 'Y';
elseif nucl == 'Sn-126'
      n = 11; anion = 'Y';
elseif nucl == 'Sr-90 '
      n = 12; anion = 'N';
elseif nucl == 'Tc-99 '
      n = 13; anion = 'N';    % (Tc is anion in oxidising conditions)
elseif nucl == 'Zr-93 '
      n = 14; anion = 'N';
elseif nucl == 'Zr-93f'
      n = 14; anion = 'N';
end

nucl = sscanf(nucl,'%s');     % renaming (a string without blanks)
% ------------------------------------------------------------
```

```
% ------------------------------------------------------------
% K_d = retardation coefficient (m^3/kg)
% (K_a = surface retardation coefficient (m^3/m^2))
% (TILA-99, Table 11-9, p.118):
% according to the alphabetical nuclide name order
% and the salinity condition order
% ------------------------------------------------------------

%--------------------------------
%      non-sal  saline  nuclide
%--------------------------------
K_ds =[0.0001   0.0001; % C-14
       0        0;      % Cl-36
       0.05     0.01;   % Cs-135
       0.05     0.01;   % Cs-137
       0        0;      % I-129
       0.02     0.02;   % Nb-94
       0.1      0.005;  % Ni-59
       0.1      0.005;  % Ni-63
       0.001    0.0001; % Pd-107
       0.0005   0.0001; % Se-79
       0.001    0.0001; % Sn-126
       0.005    0.0001; % Sr-90
       0.05     0.05;   % Tc-99
       0.2      0.2;];  % Zr-93

K_d = K_ds(n,sal);
K_a = 0;    % K_a is not incorporated in the same model as K_d
% ------------------------------------------------------------
% ------------------------------------------------------------
% e_p = rock porosity (-)
% D_e = effective diffusion coefficient to the rock matrix (m^2/s)
% e_p, D_e (TILA-99, Table 11-10, p. 120):
% according to the value of K_d, anion status of the nuclide,
% and salinity conditions
% ------------------------------------------------------------

if K_d > 1e-4
   dist = '0';     % distance to the matrix 0-1 cm
else
   dist = '1';     % distance to the matrix 1-10 cm
end

% [e_p] = (-)
e_N_1_0 = 0.5d-2;  % Non-anions, non-saline, distance = 0-1 cm
e_N_1_1 = 0.1d-2;  % Non-anions, non-saline, distance = 1-10 cm

e_N_2_0 = 0.5d-2;  % Non-anions, saline, distance = 0-1 cm
e_N_2_1 = 0.1d-2;  % Non-anions, saline, distance = 1-10 cm

e_Y_1_0 = 0.1d-2;  % Anions, non-saline, distance = 0-1 cm
e_Y_1_1 = 0.02d-2; % Anions, non-saline, distance = 1-10 cm

e_Y_2_0 = 0.2d-2;  % Anions, saline, distance = 0-1 cm
e_Y_2_1 = 0.04d-2; % Anions, saline, distance = 1-10 cm

% [D_e] = (m^2/s)
De_N_1_0 = 1d-13;  % Non-anions, non-saline, distance = 0-1 cm
De_N_1_1 = 1d-14;  % Non-anions, non-saline, distance = 1-10 cm

De_N_2_0 = 1d-13;  % Non-anions, saline, distance = 0-1 cm
De_N_2_1 = 1d-14;  % Non-anions, saline, distance = 1-10 cm

De_Y_1_0 = 1d-14;  % Anions, non-saline, distance = 0-1 cm
De_Y_1_1 = 1d-15;  % Anions, non-saline, distance = 1-10 cm

De_Y_2_0 = 5d-14;  % Anions, saline, distance = 0-1 cm
De_Y_2_1 = 5d-15;  % Anions, saline, distance = 1-10 cm
```

```
% 'quantity'_'anion value'_'salinity'_'distance'
e_p_name = sprintf('e_%s_%d_%s', anion, sal, dist);
De_name = sprintf('De_%s_%d_%s', anion, sal, dist);

e_p = eval(e_p_name);
D_e = eval(De_name)*365*24*3600; % [D_e] = (m^2/a)
% ------------------------------------------------------------

% ------------------------------------------------------------
% T_half (TILA-99, Table 2-3, p.21):
% according to the alphabetical nuclide name order

         % C-14   Cl-36  Cs-135 Cs-137 I-129  Nb-94  Ni-59
T_halfs = [5.7d+3 3.0d+5 2.3d+6 3.0d+1 1.6d+7 2.0d+4 8.0d+4 ...
           9.6d+1 6.5d+6 6.4d+4 1.0d+5 2.9d+1 2.1d+5 1.5d+6]; % a
         % Ni-63  Pd-107 Se-79  Sn-126 Sr-90  Tc-99  Zr-93
T_half = T_halfs(n);
% ------------------------------------------------------------
```

```
% ------------------------------------------------------------------
% Calculation of the output of a rectangular input as a difference of
% outputs of two step inputs.
% Solution for a constant inlet condition: eq. (77)
% ------------------------------------------------------------------
% Last modification 9.11.1999
% ------------------------------------------------------------------

function C = C_out(A, t0, lambda, R_f, C0, DT, T, N_DTi)

% -------------------------------------------------------
% Calculation of the output of the positive input
% -------------------------------------------------------

T1 = T;

for i = 1:length(T1);
   C1(i) = 0.5*exp(-lambda*(t0)) * ...
      (exp(-sqrt(lambda)*(t0/A)) * ...
      erfc(t0/(2*A*sqrt(T1(i)-t0))-sqrt(lambda*(T1(i)-t0))) + ...
      exp(sqrt(lambda)*(t0/A)) * ...
      erfc(t0/(2*A*sqrt(T1(i)-t0))+sqrt(lambda*(T1(i)-t0))));
end

% -------------------------------------------------------
% Calculation of the output of the negative input
% -------------------------------------------------------

T2 = T1(N_DTi+1:length(T1))-DT;

for i = 1:length(T2);
   if T2(i) <= t0 % pulse not reached the measuring distance
   C2(i) = 0;
   else
   C2(i) = 0.5*exp(-lambda*(t0)) * ...
      (exp(-sqrt(lambda)*(t0/A)) * ...
      erfc(t0/(2*A*sqrt(T2(i)-t0))-sqrt(lambda*(T2(i)-t0))) + ...
      exp(sqrt(lambda)*(t0/A)) * ...
      erfc(t0/(2*A*sqrt(T2(i)-t0))+sqrt(lambda*(T2(i)-t0))));
   end
end

C2 = [zeros(1,N_DTi) C2]; % addition of N_DTi zeros in front of C2

C = C0*(C1-C2);

% remove possible negative values of C
for i = 1:length(C)
   if C(i) < 0
      C(i) = 0;
   end
end
```